НАЦІОНАЛЬНА АКАДЕМІЯ НАУК УКРАЇНИ
ІНСТИТУТ ЗАГАЛЬНОЇ ТА НЕОРГАНІЧНОЇ ХІМІЇ імені В. І. ВЕРНАДСЬКОГО
КИЇВСЬКИЙ НАЦІОНАЛЬНИЙ УНІВЕРСИТЕТ імені ТАРАСА ШЕВЧЕНКА

УКРАЇНСЬКИЙ ХІМІЧНИЙ ЖУРНАЛ

№ 3
Том 91 / Vol. 91
2025
https://ucj.org.ua

UKRAINIAN CHEMISTRY JOURNAL

Зміст

Contents

УДК 546.224-31:547.233:547.477.1 doi: 10.33609/2708-129X.91.3.2025.3-24

SULFUR DIOXIDE INTERACTION WITH MONOETHANOLAMMONIUM AND POLYETHYLENEPOLYAMMONIUM CITRATES AQUEOUS SOLUTIONS PRODUCTS COMPOSITION AND THE RELATIVE STABILITY.

R. E. Khoma*, K. V. Tsyganenko, T. S. Bienkovska, Yu. V. Ishkov, S. V. Vodzinskii

Odessa I.I. Mechnikov National University,
2 Dvoryanska str., 65082 Odessa, Ukraine
**e-mail: rek@onu.edu.ua*

The paper presents the results of pH, redox, and conductometric studies on the acid-base interaction during sulfur dioxide chemisorption by aqueous solutions containing 0.1 mol/L monoethanolammonium **(MEA·1/3CA)** and polyethylenepolyammonium **(PEPA·1/3CA)** citrates, as well as buffer solutions of monoethanolamine – monoethanolammonium citrate **(MEA·1/6CA)**and polyethylenepolyamine – polyethylenepolyammonium citrate **(PEPA·1/6CA)**, in comparison with sodium citrate. The composition of the compounds formed during SO_2 absorption by Na_3Cit, MEA·1/3CA, PEPA·1/3CA, MEA·1/6CA, and PEPA·1/6CA solutions at 273–313 K was determined. For the same amount of absorbed sulfur dioxide, an increase in specific electrical conductivity (æ) with rising temperature was observed in SO_2–Na_3Cit–H_2O and SO_2–MEA·1/3CA–H_2O solutions within the 273–313 K range. However, in the SO_2–MEA·1/3CA–H_2O, SO_2–PEPA·1/3CA–H_2O, SO_2–MEA·1/6CA–H_2O, and SO_2–PEPA·1/6CA–H_2O systems, a decrease in Δæ was noted upon heating to 303 K, which is attributed to their ion-molecular composition.

Based on developed mathematical models, the ion-molecular component composition of SO_2–MEA·1/3CA–H_2O and SO_2–MEA·1/6CA–H_2O solutions was determined at 283–313 K. The concentration and thermodynamic constants for the formation of ionic associates were calculated:
$(\overset{+}{N}H_3CH_2CH_2OH)_2SO_3$, $\{\overset{+}{N}H_3CH_2CH_2OH\}\{HOC_3H_4(COOH)_2(COO^-)\}$ (**Ia**),
$\{\overset{+}{N}H_3CH_2CH_2OH\}_2\{HOC_3H_4(COOH)(COO^-)_2\}$ (**IIa**),
$\{\overset{+}{N}H_3CH_2CH_2OH\}_2\{HOC_3H_4(COOH)_2(COO^-)\}$ (**IIb**),
$\{\overset{+}{N}H_3CH_2CH_2OH\}_3\{HOC_3H_4(COO^-)_3\}$ (**IIIa**),
as well as ion-molecular associates:
$\{\overset{+}{N}H_3CH_2CH_2OH\}\{HOC_3H_4(COOH)_3\}$ (**Ib**),
$\{NH_2CH_2CH_2OH\}_3\{\overset{+}{N}H_3CH_2CH_2OH\}_3\{HOC_3H_4(COO^-)_3\}$ (**IVa**),
$\{NH_2CH_2CH_2OH\}_2\{\overset{+}{N}H_3CH_2CH_2OH\}_4\{HOC_3H_4(COO^-)_3\}$ (**IVb**).

In SO_2–MEA·1/3CA–H_2O solutions, as the temperature increases, bond rearrangement occurs in ionic associates **IIa** and **Ib**, as indicated by the absence of a clear temperature dependence of p β^T_{IIIa}, along with the strengthening of **IIa** and **Ib**. Conversely, in SO_2–MEA·1/6CA–H_2O solutions, increasing temperature leads to the weakening of the bonds in compounds **Ia, IIIa, IVa,** and **IVb**, while in compound **Ib,** the bonds strengthen.

Keywords: sulfur dioxide, ammonium citrates, acid-base interaction, ion associates, ion-molecular associates.

INTRODUCTION. For sanitary air purification from acidic gases (particularly SO_2), absorption and adsorption methods using various chemisorbents are widely used [1, 2]. Previously, the authors [3, 4] studied the acid-base interaction of sulfur dioxide with model aqueous solutions of organic N-containing bases (**AM**), including monoethanolamine (**MEA**) and polyethylenepolyamine (**PEPA**), to develop chemisorbents for acidic gas filtration in respiratory protection [3–5]. To prevent the evaporation of volatile MEA from the surface of impregnated fibrous chemisorbents (**IFCS**) under the flow of a gas-air mixture, polybasic acids (particularly citric acid (**CA**)) were added to the impregnating aqueous solutions based on MEA. This modification enhanced the protective characteristics of IFCS against SO_2 exposure [5]. Additionally, aqueous sodium citrate solutions ($HOC(CH_2COONa)_2COONa$; **Na_3Cit**) have been identified as effective chemisorbents for this gas [6–8].

Methods of pH-, redox- and conductometric titration have been successfully applied to determine the reactivity of model aqueous AM solutions towards SO_2 and CA, allowing for the calculation of their ion-molecular composition and formation constants of weakly dissociated compounds (such as ammonium sulfites, hydrosulfites, pyrosulfites; and ion-molecular complexes) [3, 4, 9].

In [9] the acid-base and electrochemical behavior of Na_3Cit – CA – H_2O, MEA – CA – H_2O, and PEPA – CA – H_2O solutions were analyzed using pH-metric and conductometric data. The study determined the influence of amine type and temperature on the ionic-molecular composition, ionic strength, and structural characteristics of these systems. It also identified key factors (component ratios and temperature) affecting the formation constants of ionic associates. In [10], the influence of water content and **MEA** on the physical and chemical adsorption of sulfur dioxide by **IFCS** samples based on citrate-monoethanolammonium buffer systems was investigated. Competitive adsorption of H_2O and SO_2 by the surface of the indicated **IFCS** was noted. However, no comprehensive data exists in the literature regarding the interaction of sulfur dioxide with ammonium citrates.

Given this gap, the present study aims to determine the composition and relative stability of the products formed during the interaction of sulfur dioxide with aqueous solutions of sodium citrate, monoethanolammonium citrate (**MEA·1/3CA**), and polyethylenepolyammonium citrate (**PEPA·1/3CA**), as well as with buffer solutions of monoethanolamine – monoethanolammonium citrate (**MEA·1/6CA**) and polyethylenepolyamine – polyethylenepolyammonium citrate (**PEPA·1/6CA**). To achieve this goal, a pH, redox, and conductometric study of the above interactions was carried out.

EXPERIMENT AND DISCUSSION OF RESULTS. In this study, monoethanolamine (MEA), sodium citrate (Na_3Cit), and citric acid (CA) of "chemically pure" classification, as well as polyethylenepolyamine (PEPA) (CAS 29320-38-5) without preliminary purification were used. Their characteristics are given in Table 1. Additionally, gaseous sulfur dioxide was supplied from a cylinder. As chemisorbents, aqueous solutions of Na_3Cit, MEA·1/3CA, MEA·1/6CA, PEPA·1/3CA, and PEPA·1/6CA with a Na^+ ion or amine nitrogen concentration of 0.1 mol/L were used. Aqueous solutions of MEA·1/3CA and MEA·1/6CA were prepared by adding a CA solution to an MEA solution at a molar ratio of components

of 1.0:3.0 and 1.0:6.0, respectively. Aqueous solutions of PEPA·1/3CA and PEPA·1/6CA were prepared similarly. The procedure for pH-, redox- and conductometric titration of aqueous solutions with gaseous sulfur dioxide is described in detail in [20].

Figures 1–8 present the pH, redox, and conductometric titration curves for 0.1 mol/L aqueous solutions of Na_3Cit, MEA·1/3CA, PEPA·1/3CA, MEA·1/6CA and PEPA·1/6CA with gaseous sulfur dioxide.

On the integral pH-metric titration curves (Fig. 1, 2) of aqueous solutions of sodium citrates, monoethanolammonium, and polyethylenepolyammonium with gaseous sulfur dioxide, a single jump is observed at the molar ratios $Q(SO_2):Q(Na) = (0.86 \div 0.97):2.00$, $Q(SO_2):Q(N_{MEA}) = (0.92 \div 0.98):2.00$ and $Q(SO_2):Q(N_{PEPA}) = (0.63 \div 0.81):2.00$. These correspond to the peaks on the differential curves (see, for example, Fig. 4a) and contrast with the MEA and PEPA solutions [3], which exhibit two effects.

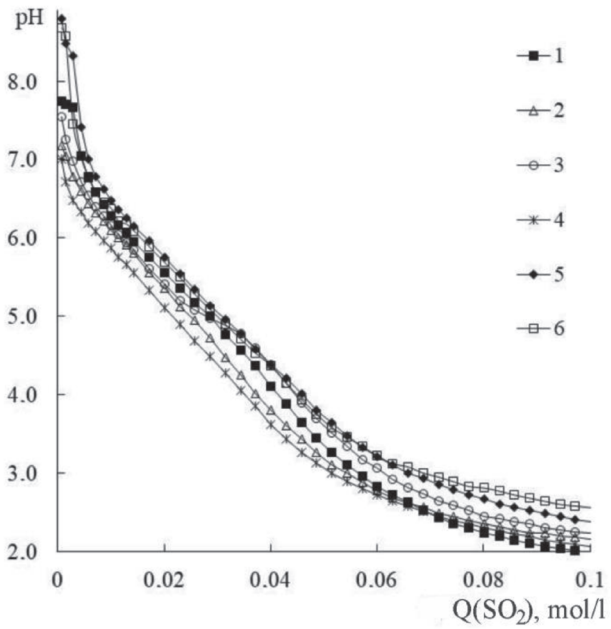

Fig. 1. Integral pH-metric titration curves of a 0.1 mol/L Na_3Cit aqueous solution with gaseous SO_2 at different temperatures (T, K): 273 – 1; 283 – 2; 293 – 3; 298 – 4; 303 – 5; 313 – 6.

This behavior is due to the weakly alkaline nature of the initial citrate solutions (Fig. 1–2; pH 7.61 ÷ 8.82 (Na_3Cit), 6.32 ÷ 6.50 (MEA·1/3CA), and 4.80 ÷ 5.42 (PEPA·1/3CA)). The observed effects on the differential curves occur in an acidic environment (Table 2; pH 3.60 ÷ 3.94 (Na_3Cit), 3.30 ÷ 3.96 (MEA·1/3CA) and 2.81 ÷ 3.74 (PEPA·1/3CA)) and are associated with the formation of hydrosulfites of the corresponding cations. Deviations of the $Q(SO_2):Q(Na)$, $Q(SO_2):Q(N_{MEA})$, and $Q(SO_2):Q(N_{PEPA})$ ratios from the stoichiometry value (1.00:2.00) are due to additional interactions, particularly the stepwise protonation of citrate ions in the specified pH range [9, 20].

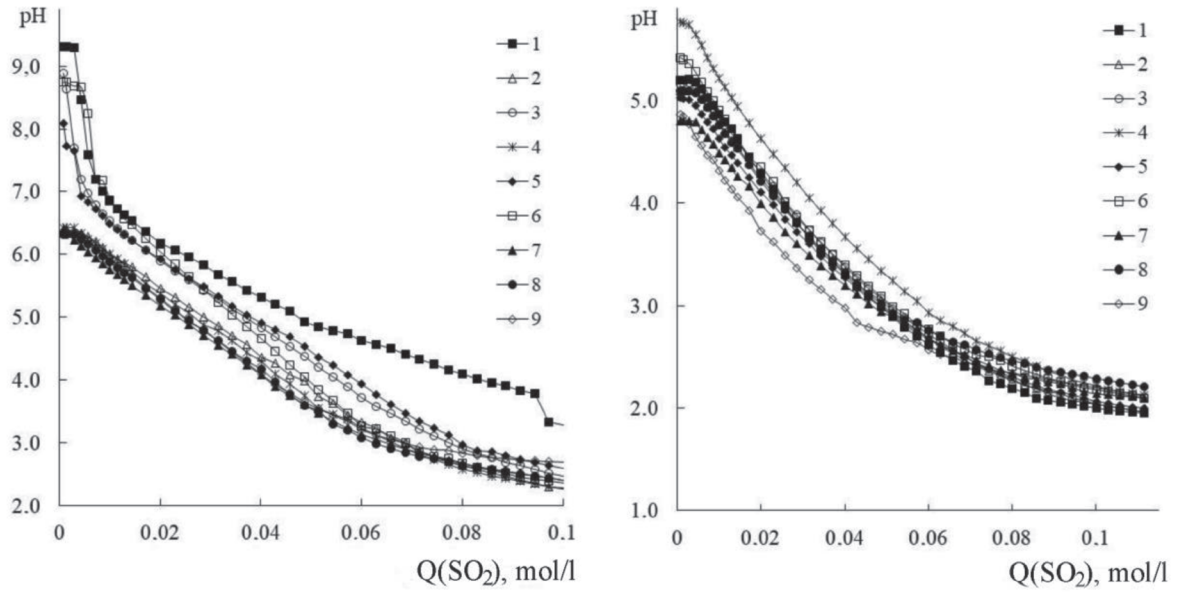

a *b*

Fig. 2. Integral pH-metric titration curves of a 0.1 mol/L MEA·1/3CA (*a*) and PEPA·1/3CA (*b*) aqueous solution with gaseous SO_2 at different temperatures (T, K): 273 – 1; 278 – 2; 283 – 3; 288 – 4; 293 – 5; 298 – 6; 303 – 7; 308 – 8; 313 – 9.

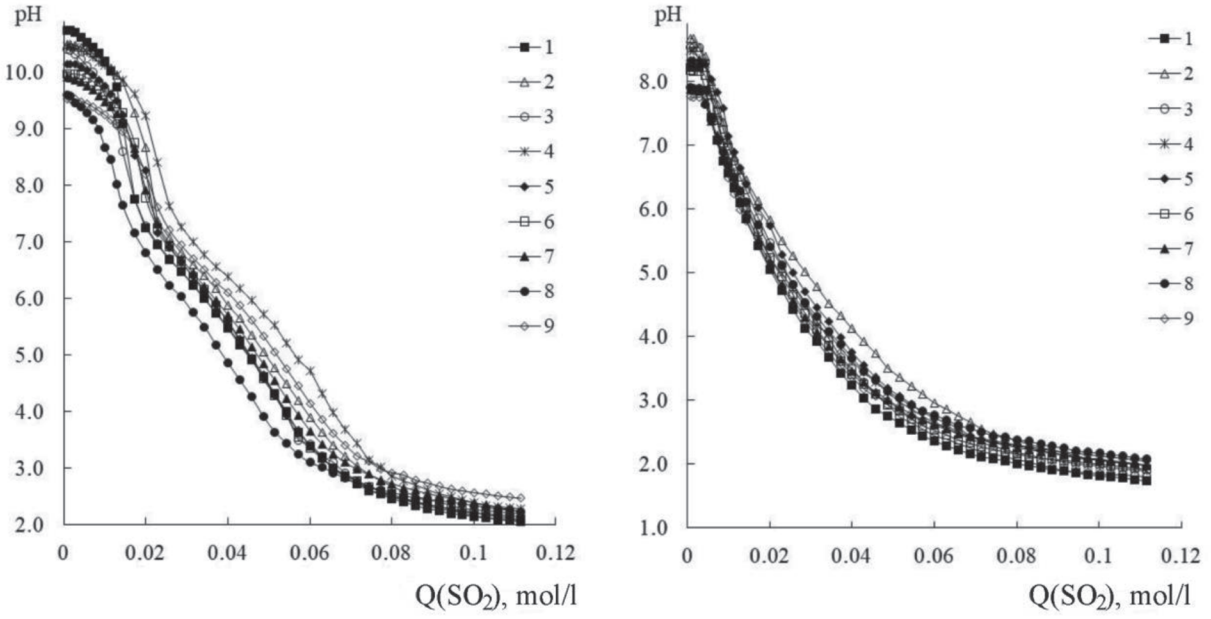

a *b*

Fig. 3. Integral pH-metric titration curves of MEA·1/6CA (*a*) and PEPA·1/6CA (*b*) aqueous solutions with gaseous SO_2 at different temperatures (T, K): 273 – 1; 278 – 2; 283 – 3; 288 – 4; 293 – 5; 298 – 6; 303 – 7; 308 – 8; 313 – 9.

Table 1.

Physicochemical characteristics of the starting compounds.

Name	**Citric acid**	**Sodium citrate**	**Mono-ethanolamine**	**Polyethylene polyamine**
Designation	**CA**	**Na_3Cit**	**MEA**	**PEPA**
Structural formula	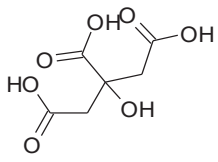	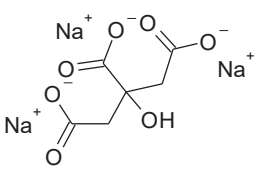	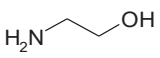	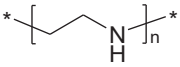
General formula	$HOC_3H_4(COOH)_3$	$HOC_3H_4(COONa)_3$	$NH_2CH_2CH_2OH$	NH_2-$(CH_2CH_2NH)_k$-H
M, g/mol	192.12	258.06	61.08	42.0
pK_a	3.13; 4.76; 6.39 [12]	3.13; 4.76; 6.39 [12, 16]	9.20 [1]	9.21 [18]
Melting point, °C	153 [12, 13]	300 [16]	10.5 [1, 17]	-32.0 [18, 19]
Boiling point, °C	310 [14]	–	170.3 [1, 17]	Decompos. [18, 19]
P, Pa (20 ^{0}C)	$2.21 \cdot 10^{-6}$ [13]	0	53 [1, 17]	<1.33 [18, 19]
lg$P$	-1.64 [15]	-1.72 [16]	-1.31 [1, 17]	-3.67 [18, 19]

In the case of MEA·1/6CA solutions, two jumps are observed on the integral pH-metric curves (Fig. 3a; Table 2) and two maxima on the differential pH-metric curves (e.g., Fig. 4b) at the ratios $Q(SO_2):Q(N_{MEA})$ = (0.34 ÷ 0.52):2.00 and (0.49 ÷ 0.63):1.00. In contrast, PEPA·1/6CA solutions (Fig. 3b; Table 2) exhibit only one effect on the corresponding curves at $Q(SO_2):Q(N_{PEPA})$ = (0.68 ÷ 0.86):2.00. This difference arises from the more alkaline nature of the initial MEA·1/6CA solutions (pH 9.53 ÷ 9.74) compared to PEPA·1/6CA solutions (pH 7.76 ÷ 8.67).

Analyzing the data shown in Fig. 1-3, the pH values of chemisorption systems at 293 K can be arranged in the following sequence:

– for $Q(SO_2) < 0.02$ mol/L MEA·1/6CA > PEPA·1/6CA > MEA·1/3CA > Na_3Cit > PEPA·1/3CA;

– for $0.02 < Q(SO_2) < 0.05$ mol/L MEA·1/6CA > MEA·1/3CA > Na_3Cit > PEPA·1/6CA > PEPA·1/3CA;

– for $0.05 < Q(SO_2) < 0.10$ mol/L MEA·1/3CA > MEA·1/6CA ≥ Na_3Cit > PEPA·1/6CA ≥ PEPA·1/3CA.

These results indicate that at SO_2 concentrations above 0.05 mol/L, solutions based on monoethanolammonium citrate exhibit the highest efficiency in binding this toxicant.

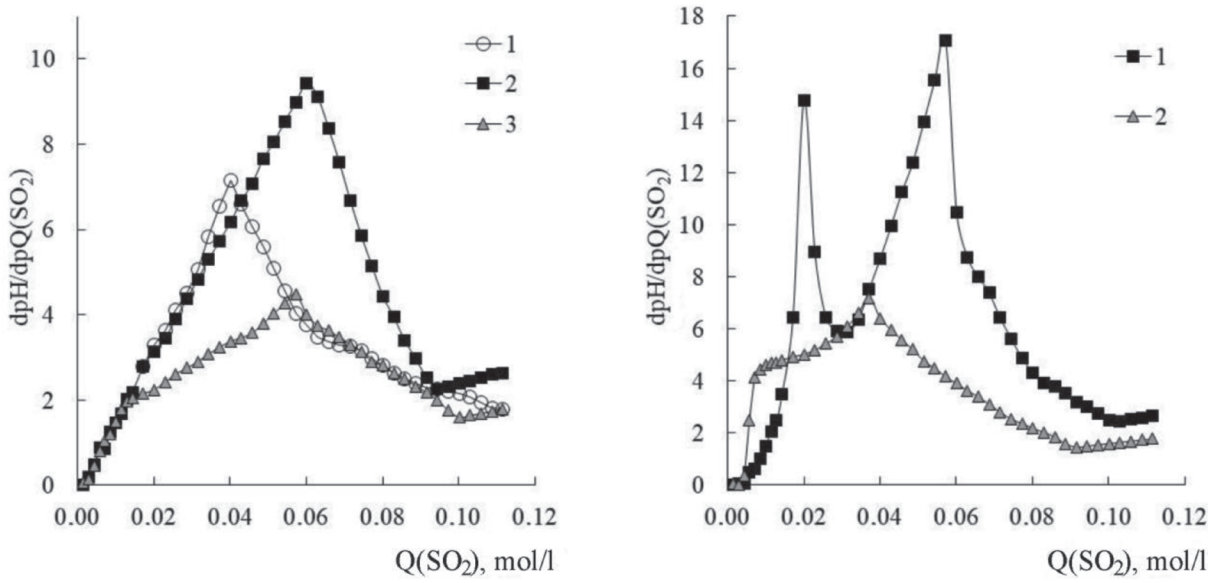

a *b*

Fig. 4. Differential pH-metric titration curves of 0.1 M Na_3Cit (1*a*), MEA·1/3CA (2*a*), PEPA·1/3CA (3*a*), MEA·1/6CA (1*b*) and PEPA·1/6CA (2*b*) aqueous solutions with gaseous SO_2 at 298 K.

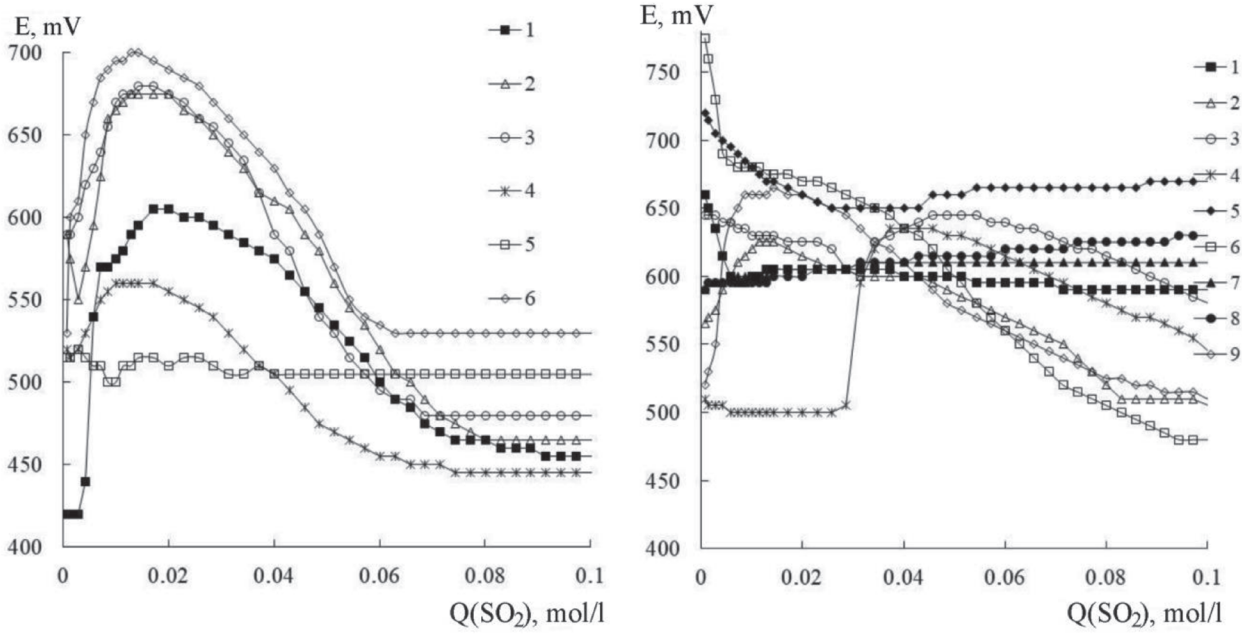

a *b*

Fig. 5. Redox-metric titration curves of 0.1 mol/L Na_3Cit (*a*) and MEA·1/3CA (*b*) aqueous solutions with gaseous SO_2 at different temperatures (T, K): 273 – 1; 283 – 2; 293 – 3; 298 – 4; 303 – 5; 313 – 6.

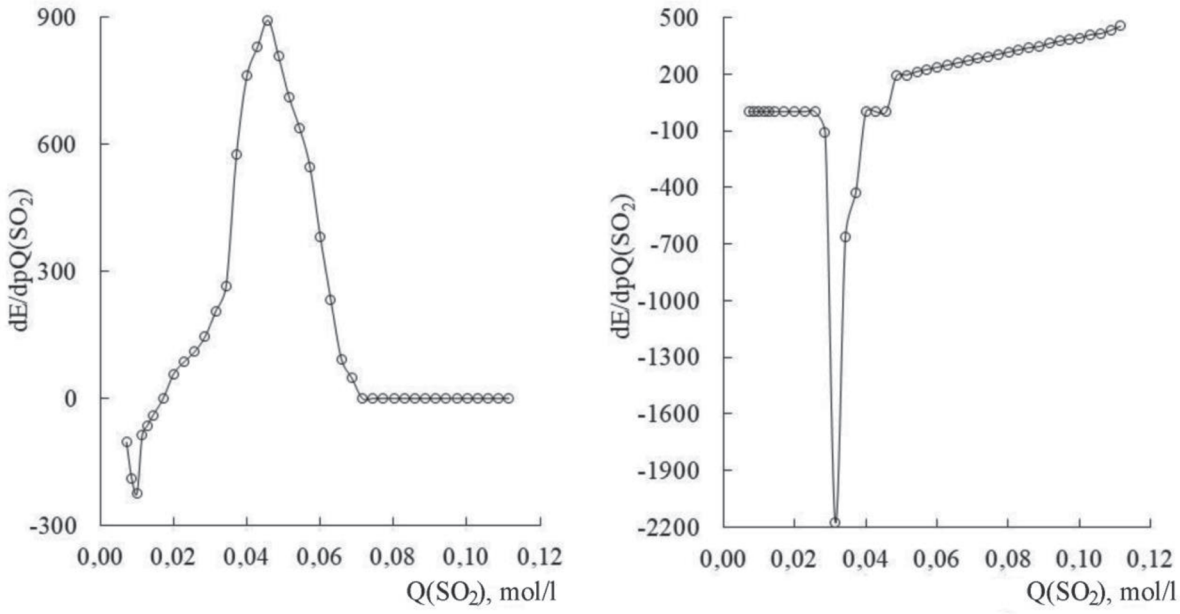

a *b*

Fig. 6. Differential Redox-metric titration curves of 0.1 mol/L Na_3Cit (*a*) and MEA·1/3CA (*b*) aqueous solutions with gaseous SO_2 at 288 K (*b*), and 293 K (*a*).

Negative Δæ values suggest the formation of weakly dissociated compounds in the SO_2 – Na_3Cit – H_2O, SO_2 – MEA·1/3CA – H_2O, and SO_2 – MEA·1/6CA – H_2O systems (Fig. 7 – 9; Table 3). In PEPA-containing solutions, positive Δæ values ($Q(SO_2) > 0.05$ mol/L; T = 273 – 283 K) indicate an increase in the degree of dissociation of existing species (H_2O, $SO_2 \cdot H_2O$, HSO_3^-), the formation of new strongly dissociated compounds, and an increase in the mobility of newly formed ions [3, 11, 20], as discussed below.

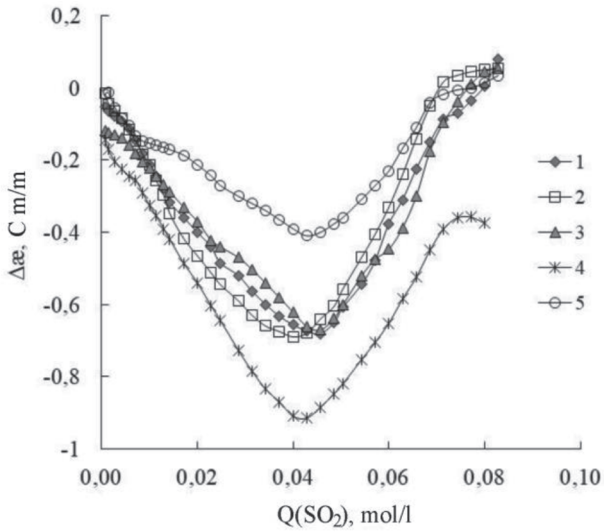

Fig. 7. Conductometric titration curves of 0.1 M Na_3Cit aqueous solutions with gaseous SO_2 at different temperatures (T, K): 273 – 1; 283 – 2; 293 – 3; 303 – 4; 313 – 5.

In the SO_2 – MEA·1/3CA – H_2O system (Fig. 8a; Table 3), the relative decrease in Δæ with increasing sulfur dioxide content up to 0.040 mol/L (at 303, 283 K) and 0.050 mol/L (at 273, 278, 293, and 313 K) is attributed to the formation of monoethanolammonium sulfite, similar to findings in [3, 20]. Further increases in $Q(SO_2)$ are accompanied by a relative increase in the specific electrical conductivity, driven by the formation of monoethanolammonium hydrosulfite and pyrosulfite. As the temperature increases within the 283–303 K range, a relative decrease in Δæ is observed at the same $Q(SO_2)$ values in the 0.01 ÷ 0.05 mol/L region.

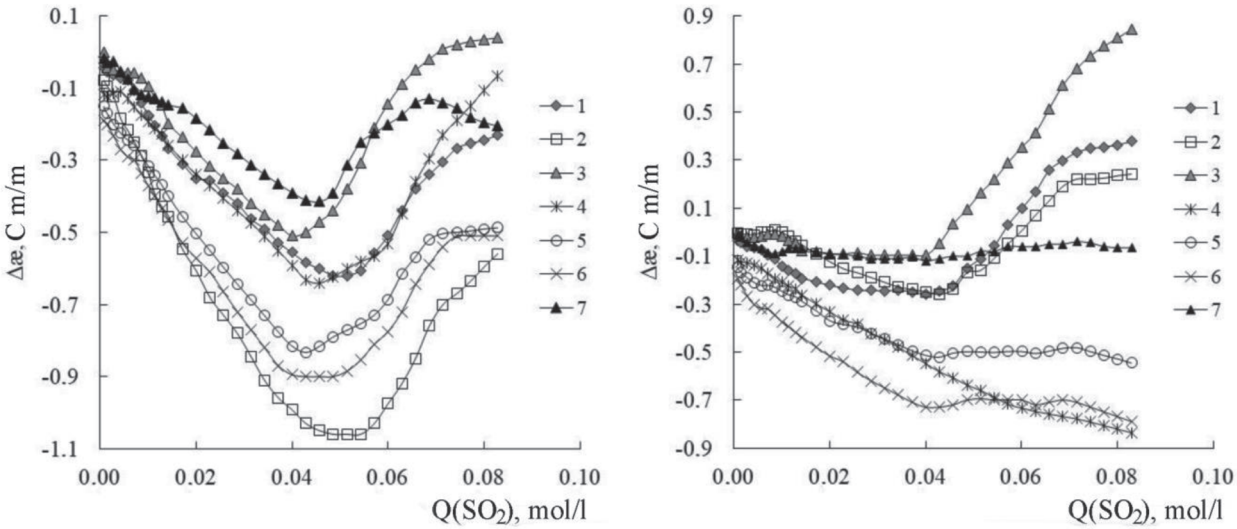

a *b*

Fig. 8. Conductometric titration curves of 0.1 M MEA·1/3CA (*a*), and PEPA·1/3CA (*b*) aqueous solutions with gaseous SO_2 at different temperatures (T, K): 273 – 1; 278 – 2; 283 – 3; 293 – 4; 298 – 5; 303 – 6; 313 – 7.

Table 2.

Characteristics of pH-metric titration curves of Na_3Cit, MEA·1/3CA, PEPA·1/3CA, MEA·1/6CA, and PEPA·1/6CA aqueous solutions with gaseous SO_2.

T, K	1st maximum			2nd maximum		
	$Q(SO_2)$: Q(Na/N)	pH	dpH/dpQ(SO_2)	$Q(SO_2)$: Q(Na/N)	pH	dpH/dpQ(SO_2)
			Na_3Cit			
273	0.429	3.88	8.21	–	–	–
283	0.429	3.60	7.32	–	–	–
293	0.476	3.90	8.56	–	–	–
298	0.404	3.62	7.15	–	–	–
303	0.486	3.81	7.60	–	–	–
313	0.476	3.94	7.49	–	–	–

T, K	1st maximum			2nd maximum		
	$Q(SO_2) : Q(Na/N)$	pH	$dpH/dpQ(SO_2)$	$Q(SO_2) : Q(Na/N)$	pH	$dpH/dpQ(SO_2)$
			MEA·1/3CA			
273	0.472	3.78	13.47	–	–	–
278	0.472	3.78	18.71	–	–	–
283	0.458	3.96	14.51	–	–	–
288	0.472	3.55	14.97	–	–	–
293	0.486	3.30	18.51	–	–	–
298	0.458	3.61	13.33	–	–	–
303	0.472	3.47	10.48	–	–	–
308	0.486	3.30	15.43	–	–	–
313	0.458	3.65	10.15	–	–	–
			PEPA·1/3CA			
273	0.404	3.30	3.73	0.543	2.79	4.26
278	0.315	3.66	3.62	0.515	2.94	4.43
283	0.315	3.74	3.62	0.515	2.97	4.03
288	0.572	3.04	4.48	–	–	–
293	0.458	3.07	3.57	–	–	–
298	0.572	2.82	4.49	–	–	–
303	0.543	2.81	3.41	–	–	–
308	0.515	2.92	4.03	–	–	–
313	0.343	3.16	2.90	–	–	–
			MEA·1/6CA			
273	0.172	7.75	16.92	0.572	3.64	16.61
278	0.200	8.67	8.96	0.601	3.9	14.16
283	0.172	7.75	10.74	0.572	3.5	21.10
288	0.258	7.63	15.05	0.629	4.32	19.80
293	0.200	8.26	18.97	0.543	3.94	15.33
298	0.200	7.77	14.79	0.486	4.58	13.67
303	0.200	7.91	10.91	0.572	3.94	13.02
308	0.129	8.02	8.41	0.486	3.92	12.91
313	0.229	7.61	10.0	0.601	4.15	14.16
313	0.343	3.16	2.90	–	–	–
			PEPA·1/6CA			
273	0.372	3.42	7.48	–	–	–
278	0.486	3.51	8.36	–	–	–
283	0.372	3.68	8.34	–	–	–
288	0.315	4.18	7.25	–	–	–
293	0.372	3.98	7.48	–	–	–
298	0.372	3.61	7.19	–	–	–
303	0.429	3.28	6.01	–	–	–
308	0.404	3.66	6.84	–	–	–
313	0.3432	3.75	6.35	–	–	–

Table 3.

Characteristics of conductometric titration curves of MEA·1/3CA, PEPA·1/3CA, MEA·1/6CA, and PEPA·1/6CA aqueous solutions.

T, K	I-th effect		II-th effect		III-th effect		IV-th effectr	
	$Q(SO_2) : Q(N)$ (*curve shape*)	Δæ, Cm/m	$Q(SO_2) : Q(N)$ (*curve shape*)	Δæ, Cm/m^{-1}	$Q(SO_2) : Q(N)$ (*curve shape*)	Δæ, Cm/m^{-1}	$Q(SO_2) : Q(N)$ (*curve shape*)	Δæ, Cm/m^{-1}
MEA·1/3CA								
273	0.200 (bend)	-0.35	0.510 (bend)	-0.608	0.740 (bend)	-0.276	–	–
278	0.480 (bend)	-1.06	0.540 (bend)	-1.060	0.710 (bend)	-0.760	–	–
283	0.071 (bend)	-0.06	0.400 (min)	-0.510	0.710 (bend)	0.020	–	–
293	0.043 (bend)	-0.114	0.457 (min)	-0.640	0.570 (bend)	-0.565	–	–
298	0.428 (min)	-0.833	0.570 (bend)	-0.729	0.714 (bend)	-0.503	–	–
303	0.400 (bend)	-0.895	0.510 (bend)	-0.885	0.740 (bend)	-0.510	–	–
313	0.171 (bend)	-0.156	0.457 (min)	-0.415	0.686 (bend)	-0.130	–	–
PEPA·1/3CA								
273	0.143 (bend)	-0.192	0.404 (min)	-0.258	0.715 (bend)	0.332	–	–
278	0.072 (max)	0.002	0.429 (min)	-0.259	0.715 (bend)	0.221	–	–
283	0.057 (bend)	-0.017	0.143 (bend)	-0.078	0.400 (bend)	-0.096	0.744 (bend)	0.734
293	0.572 (bend)	-0.717	–	–	–	–	–	–
298	0.572 (bend)	-0.222	0.429 (min)	-0.520	0.486 (bend)	-0.498	0.629 (bend)	-0.506
303	0.400 (min)	-0.729	0.486 (bend)	-0.699	0.686 (bend)	-0.700	–	–
313	0.086 (min)	-0.090	0.129 (max)	-0.070	0.286 (bend)	-0.110	0.400 (bend)	-0.12
MEA·1/6CA								
273	0.110 (max)	0.026	0.486 (min)	-0.38	0.714 (bend)	0.134	–	–
278	0.110 (min)	0.086	0.466 (bend)	-0.38	0.514 (min)	-0.520	0.714 (bend)	-0.030
283	0.100 (max)	0.220	0.486 (min)	-0.21	0.714 (bend)	0.160	–	–
293	0.170 (max)	0.040	0.514 (min)	-0.29	0.714 (bend)	0.140	–	–
298	0.428 (min)	-0.215	0.200 (max)	-0.074	0.486 (min)	-0.480	0.714 (bend)	-0.043
303	0.043 (min)	-0.270	0.710 (max)	-0.24	0.151 (bend)	-0.280	0.540 (bend)	-0.780
313	0.071 (min)	-0.070	0.020 (max)	0.04	0.543 (min)	-0.200	0.628 (bend)	-0.20
PEPA·1/6CA								
273	0.143 (bend)	-0.248	0.468 (min)	-0.432	0.743 (bend)	-0.182	–	–
278	0.071 (bend)	-0.013	0.310 (bend)	-0.236	0.400 (bend)	-0.236	0.743 (bend)	0.434
283	0.100 (bend)	-0.068	0.143 (bend)	-0.015	0.400 (min)	-0.231	0.710 (bend)	0.258
293	0.200 (bend)	-0.313	0.314 (bend)	-0.326	0.428 (min)	-0.381	0.743 (bend)	-0.159
298	0.143 (bend)	-0.364	0.428 (min)	-0.540	0.629 (max)	-0.396	–	–
303	0.400 (bend)	-0.701	0.714 (max)	-0.661	–	–	–	–
313	0.017 (min)	-0.123	0.129 (bend)	-0.129	0.429 (bend)	-0.148	0.571 (bend)	-0.038

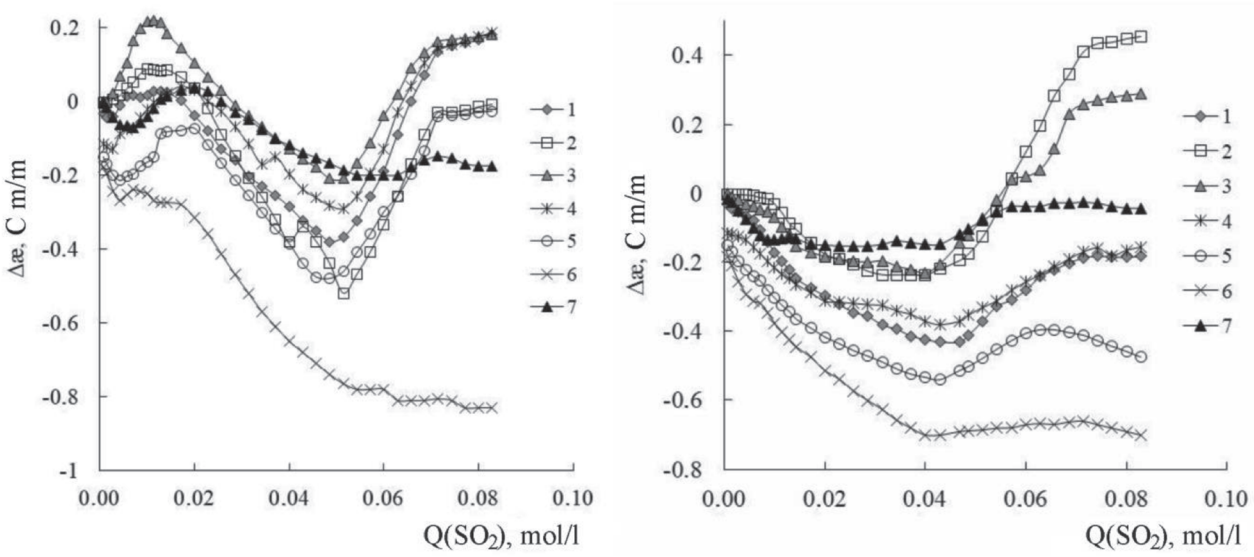

a *b*

Fig. 9. Conductometric titration curves of 0.1 mol/L MEA·1/6CA (*a*) and PEPA·1/6CA (*b*) aqueous solutions with gaseous SO_2 at different temperatures (T, K): T (K): 273 – 1; 278 – 2; 283 – 3; 293 – 4; 298 – 5; 303 – 6; 313 – 7.

At the same $Q(SO_2)$ values, an increase in σ with rising temperature (273–313 K) is observed for SO_2 – Na_3Cit – H_2O and SO_2 – MEA·1/3CA – H_2O solutions. In contrast, in SO_2 – MEA·1/3CA – H_2O, SO_2 – PEPA·1/3CA – H_2O, SO_2 – MEA·1/6CA – H_2O and SO_2 – PEPA·1/6CA – H_2O systems (Figs. 8, 9), Δæ values decrease upon heating within the 283–303 K range. his behavior is attributed to the ionic-molecular composition of the studied systems, which is discussed below.

When sulfur dioxide is absorbed by an MEA·1/6CA solution, Δæ acquires positive values (Fig. 9a) only in specific sections of the $\Delta æ = f(Q(SO_2))$ curves at: 273 K ($0.005 < Q(SO_2) < 0.020$ mol/L), 278 K ($0.002 < Q(SO_2) < 0.020$ mol/L), 283 K ($0.002 < Q(SO_2) < 0.030$ mol/L), 293 K ($0.012 < Q(SO_2) < 0.025$ mol/L) and 313 K ($0.013 < Q(SO_2) < 0.025$ mol/L). Under other experimental conditions, $\Delta æ \leq 0$ $Cm \cdot m^{-1}$. For PEPA·1/6CA solutions, Δæ values remain negative (Fig. 9b) during SO_2 chemisorption, except at T = 278 and 283 K (curves 2 and 3) when $Q(SO_2):Q(N) \geq 0.55$.

Unlike pH-metric curves (Fig. 3), conductometric curves (Fig. 9; Table 3) exhibit three or four effects. When sulfur dioxide is introduced into the MEA·1/6CA solution, a decrease in Δæ is observed within $0.020 < Q(SO_2) < 0.050$ mol/L across the studied temperature range (Fig. 9a). Further addition of SO_2 leads to a Δæ increase up to $Q(SO_2) \approx 0{,}070$ mol/L (except at T = 293 K), after which the $\Delta æ = f(Q(SO_2))$ dependencies reach stationary regions.

The addition of SO_2 to the PEPA·1/6CA solution leads to a decrease in Δæ within $0.010 < Q(SO_2) < 0.040$ mol/L across the studied

temperature range (Fig. 9b). When $Q(SO_2)$ exceeds (0.040 ÷ 0.045 mol/L), Δæ values begin to increase.

Each Δæ = $f(Q(SO_2))$ curve for SO_2 chemisorption in the studied solutions at a given temperature exhibits distinct effects (Fig. 9; Table 3).

The uniformity of acid-base and electrochemical behavior in solutions containing sodium, monoethanolammonium, and polyethylenepolyammonium citrates is confirmed by the overlapping initial sections of the dpH/dp$Q(SO_2)$ – $Q(SO_2)$ and Δæ – $Q(SO_2)$ curves (Fig. 4, 10).

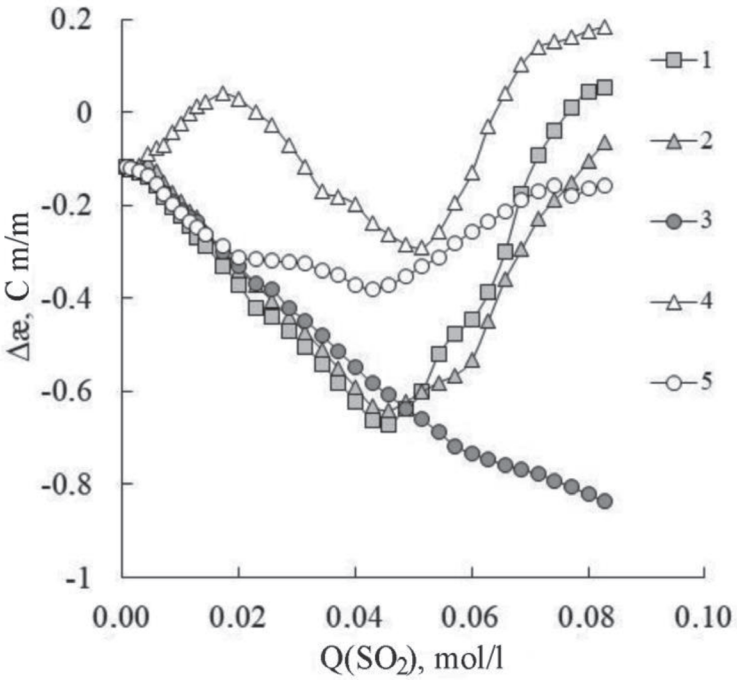

Fig. 10. Conductometric titration curves of 0.1 mol/l Na_3Cit (1), MEA·1/3CA (2) and PEPA·1/3CA (3) MEA·1/6CA (4), and PEPA·1/6CA (5) aqueous solutions with gaseous SO_2 at 293 K.

Physicochemical models of SO_2 interaction with MEA – CA – H_2O and PEPA – CA – H_2O solutions.

According to [9], in aqueous MEA·1/3CA solutions, the following processes take place: water autoprotolysis (reaction 1), MEA protonation (reaction 2), and stepwise dissociation of CA (reactions 3–5). Additionally, the formation of ionic associates occurs:

$\{\overset{+}{N}H_3CH_2CH_2OH\}\{HOC_3H_4(COOH)_2(COO^-)\}$ (**Ia**),
$\{\overset{+}{N}H_3CH_2CH_2OH\}_2\{HOC_3H_4(COOH)(COO^-)_2\}$ (**IIa**),
$\{\overset{+}{N}H_3CH_2CH_2OH\}_2\{HOC_3H_4(COOH)_2(COO^-)\}$ (**IIb**),
$\{\overset{+}{N}H_3CH_2CH_2OH\}_3\{HOC_3H_4(COO^-)_3\}$ (**IIIa**), as well as the ionic-molecular associate
$\{\overset{+}{N}H_3CH_2CH_2OH\}\{HOC_3H_4(COOH)_3\}$ (**Ib**) (reactions 6–10).

$$2H_2O \rightleftarrows H_3O^+ + OH^- \quad (1)$$

$$NH_2CH_2CH_2OH + H_3O^+ \overset{1/Ka}{\rightleftarrows} \overset{+}{N}H_3CH_2CH_2OH + H_2O \quad (2)$$

$$HOC_3H_4(COOH)_3 + H_2O \rightleftarrows HOC_3H_4(COOH)_2COO^- + H_3O^+ \quad (3)$$

$$HOC_3H_4(COOH)_2COO^- + H_2O \rightleftarrows HOC_3H_4(COOH)(COO^-)_2 + H_3O^+ \quad (4)$$

$$HOC_3H_4(COOH)(COO^-)_2 + H_2O \rightleftarrows HOC_3H_4(COO^-)_3 + H_3O^+ \quad (5)$$

$$\overset{+}{N}H_3CH_2CH_2OH + HOC_3H_4(COOH)_2(COO^-) \overset{\beta_{Ia}}{\rightleftarrows} \rightleftarrows \{\overset{+}{N}H_3CH_2CH_2OH\}\{HOC_3H_4(COOH)_2(COO^-)\} \quad (6)$$

$$\overset{+}{N}H_3CH_2CH_2OH + HOC_3H_4(COOH)_3 \overset{\beta_{Ib}}{\rightleftarrows} \rightleftarrows \{\overset{+}{N}H_3CH_2CH_2OH\}\{HOC_3H_4(COOH)_3\} \quad (7)$$

$$2\overset{+}{N}H_3CH_2CH_2OH + HOC_3H_4(COOH)(COO^-)_2 \overset{\beta_{IIa}}{\rightleftarrows} \rightleftarrows \{\overset{+}{N}H_3CH_2CH_2OH\}_2\{HOC_3H_4(COOH)(COO^-)_2\} \quad (8)$$

$$2\overset{+}{N}H_3CH_2CH_2OH + HOC_3H_4(COOH)_2(COO^-) \overset{\beta_{IIb}}{\rightleftarrows} \rightleftarrows \{\overset{+}{N}H_3CH_2CH_2OH\}_2\{HOC_3H_4(COOH)_2(COO^-)\} \quad (9)$$

$$3\overset{+}{N}H_3CH_2CH_2OH + HOC_3H_4(COO^-)_3 \overset{\beta_{IIIa}}{\rightleftarrows} \rightleftarrows \{\overset{+}{N}H_3CH_2CH_2OH\}_3\{HOC_3H_4(COO^-)_3\} \quad (10)$$

When SO_2 interacts with MEA·1/3CA – H_2O solutions, reactions 11–18 occur, leading to the formation of sulfur dioxide hydrate, sulfite, hydrosulfite, and pyrosulfite anions, as well as monoethanolammonium sulfite (**IS**), hydrosulfite (**IIS**), and pyrosulfite (**IIIS**) [3, 20].

$$SO_2^r \rightleftarrows SO_2^p \quad (11)$$

$$SO_2^p + H_2O \rightleftarrows SO_2\cdot H_2O \quad (12)$$

$$SO_2\cdot H_2O + H_2O \overset{K_1}{\rightleftarrows} H_3O^+ + HSO_3^- \quad (13)$$

$$2HSO_3^- \overset{K}{\rightleftarrows} S_2O_5^{2-} + H_2O \quad (14)$$

$$HSO_3^- + H_2O \overset{K_2}{\rightleftarrows} H_3O^+ + SO_3^{2-}, \quad (15)$$

when SO_2^r, SO_2^p – sulfur dioxide in the gas phase and dissolved in water, respectively.

$$2NH_2CH_2CH_2OH + SO_2\cdot H_2O \overset{\beta_{IS}}{\rightleftarrows} (NH_3CH_2CH_2OH)_2SO_3 \quad (16)$$

$$NH_2CH_2CH_2OH + SO_2\cdot H_2O \overset{\beta_{IIS}}{\rightleftarrows} \rightleftarrows (NH_3CH_2CH_2OH)HSO_3 \quad (17)$$

$$2NH_2CH_2CH_2OH + 2(SO_2\cdot H_2O) \overset{\beta_{IIIS}}{\rightleftarrows} \rightleftarrows (NH_3CH_2CH_2OH)_2S_2O_5 + H_2O \quad (18)$$

SO_2 – Na_3Cit – H_2O solutions

Based on [3, 4, 11, 20], the interaction of citrate ions with SO_2 hydrate results in the formation of sulfite and hydrocitrate anions (reaction 19). Additionally, the reaction of sulfite ions with SO_2 in water leads to the formation of hydrosulfite ions (reaction 20). These processes are responsible for the initial jumps observed on the pH-metric titration curves of sodium citrate aqueous solutions (Fig. 1).

$$HOC_3H_4(COO^-)_3 + SO_2\cdot H_2O + OH^- \rightarrow SO_3^{2-} + HOC_3H_4(COOH)(COO^-)_2 + H_2O \quad (19)$$

$$SO_3^{2-} + SO_2\cdot H_2O \rightarrow 2HSO_3^- \quad (20)$$

When $HOC_3H_4(COOH)(COO^-)_2$ ions interact with SO_2, hydrosulfite and dideprotonated citrate anions are formed (reaction 21). Hydrosulfite ions are also generated through the dissociation of «sulfuric» acid (reaction 13). Reactions 13 and 21 are responsible for the second jumps on the pH-metric titration curves and the minima on the conductometric curves. Additionally, at pH 4.5–6.0, hydrosulfite ion dimerization (reaction 14) leads to the formation of pyrosulfite ions, causing the first jumps on the redox-metric curves (Fig. 5*a*).

$$SO_2\cdot H_2O + HOC_3H_4(COOH)(COO^-)_2 \rightarrow HSO_3^- + HOC_3H_4(COOH)_2(COO^-) \quad (21)$$

SO_2 – MEA·1/3CA – H_2O solutions

The replacement of sodium citrate with monoethanolammonium citrate in chemisorption solutions introduces additional reactions 22–23. Alongside the reactions occurring in the SO_2 – Na_3Cit – H_2O system, this system also allows for the interaction of the ionic associate (monoethanolammonium citrate) with SO_2, which is responsible for the first jumps on the pH-metric curves (Fig. 2*a*). At pH 4,0–6,0, the reaction between SO_2 and monoethanolammonium cations in water produces an ionic associate – ammonium sulfite (reaction 23), leading to minima on the conductometric curves (Fig. 8 *a*).

$$\{\overset{+}{N}H_3CH_2CH_2OH\}_3\{HOC_3H_4(COO^-)_3\} + SO_2\cdot H_2O \rightarrow \{\overset{+}{N}H_3CH_2CH_2OH\}_2(SO_3^{2-}) + \overset{+}{N}H_3CH_2CH_2OH + HOC_3H_4(COOH)_2(COO^-) \quad (22)$$

$$2\overset{+}{N}H_3CH_2CH_2OH + SO_2\cdot H_2O + 2H_2O \rightarrow \{\overset{+}{N}H_3CH_2CH_2OH\}_2(SO_3^{2-}) + 2H_3O^+ \quad (23)$$

The multicomponent nature of SO_2 – MEA·1/3CA – H_2O solutions, resulting from the formation of H-bonded ionic associates, leads to variations in redox-metric curve shapes at different temperatures.

SO_2 – PEPA·1/3CA – H_2O solutions.

The interaction of SO_2 with polyethylenepolyammonium citrate (reaction 24) leads to the formation of polyethylenepolyammonium sulfite, polyethylenepolyamine, and dihydrocitrate ions. This process causes jumps in the pH-metric curves (Fig. 2 *b*) and breaks or minima in the conductometric curves (Fig. 8 *b*).

$$\{\overset{+}{N}H_3(CH_2CH_2\overset{+}{N}H_2)_kH\}_3\{HOC_3H_4(COO^-)_3\}_{k+1} + (k{+}1)SO_2\cdot H_2O + H_2O \rightarrow \{\overset{+}{N}H_3(CH_2CH_2\overset{+}{N}H_2)_kH\}_2(SO_3^{2-})_{k+1} + NH_2(CH_2CH_2NH)_kH + (k{+}1)HOC_3H_4(COOH)_2(COO^-) + H_3O^+ \quad (24)$$

The component composition of SO_2 – MEA·1/3CA – H_2O solutions.

Considering the law of mass action (equations 1 – 18), along with the material balance equations for nitrogen (25), citrates (26), and sulfur (27), and the electroneutrality condition (28), a system of mathematical equations (1–18, 25–28) is established.

$$Q_N = [NH_2CH_2CH_2OH] + [\overset{+}{N}H_3CH_2CH_2OH] + C_{Ia} + C_{Ib} + 2C_{IIa} + 2C_{IIb} + 3C_{IIIa} + 2C_{IS} + C_{IIS} + 2C_{IIIS} \quad (25)$$

$$Q_{Cit} = [HOC_3H_4(COOH)_3] + [HOC_3H_4(COOH)_2COO^-] + [HOC_3H_4(COOH)(COO^-)_2] + [HOC_3H_4(COO^-)_3] + C_{Ia} + C_{Ib} + C_{IIa} + C_{IIb} + C_{IIIa} \quad (26)$$

$$Q(SO_2) = [SO_2 \cdot H_2O] + [HSO_3^-] + 2[S_2O_5^{2-}] + [SO_3^{2-}] + C_{IS} + C_{IIS} + 2C_{IIIS} \quad (27)$$

$$[H^+] + [\overset{+}{N}H_3CH_2CH_2OH] + C_{Ib} + C_{IIb} = [OH^-] + [HSO_3^-] + 2[S_2O_5^{2-}] + 2\cdot[SO_3^{2-}] \quad (28)$$

where $C_{IS} = [(NH_3CH_2CH_2OH)_2SO_3]$, $C_{IIS} = [(NH_3CH_2CH_2OH)HSO_3]$,
$C_{IIIS} = [(NH_3CH_2CH_2OH)_2S_2O_5]$, $C_{Ia} = [\{\overset{+}{N}H_3CH_2CH_2OH\}\{HOC_3H_4(COOH)_2(COO^-)\}]$,
$C_{Ib} = [\{\overset{+}{N}H_3CH_2CH_2OH\}\{HOC_3H_4(COOH)_3\}]$,
$C_{IIa} = [\{\overset{+}{N}H_3CH_2CH_2OH\}_2\{HOC_3H_4(COOH)(COO^-)_2\}]$,
$C_{IIb} = [\{\overset{+}{N}H_3CH_2CH_2OH\}_2\{HOC_3H_4(COOH)_2(COO^-)\}]$,
$C_{IIIa} = [\{\overset{+}{N}H_3CH_2CH_2OH\}_3\{HOC_3H_4(COO^-)_3\}]$.

Solving this system using pH-metric data (Fig. 2 *a*) and incorporating the pK_a values of CA and MEA (Table 1) enabled the calculation of the component composition of SO_2 – MEA·1/3CA – H_2O solutions (Fig. 11).

According to the obtained data, as $Q(SO_2)$ increases from $1.4\cdot10^{-3}$ to $1.4\cdot10^{-2}$ mol/L, a rise in the relative content of monoethanolammonium cation (curve 6) is observed due to the dissociation of ionic associate **IIIa** (Fig. 11, curves 4, 7). In the region where ionic associate **IIIa** and ionic-molecular associate **IIb** form (Table 2), the total SO2 content increases the cation's partial binding into ammonium sulfite **IS** (curve 8). When ionic associate **IIb** transitions into compound **IIa** $Q(SO_2) > 0.26$ mol/L, the relative content of IS decreases (curve 8), while the binding of monoethanolamine and citrate in **IIa** increases sharply (curves 4 and 7). Across the calculated section of the pH = $f(Q(SO_2))$ curve, a rise in the molar fraction of hydrosulfite ions (curve 9; $Q(SO_2) > 0.01$ mol/L) is observed, along with a decrease in ammonium sulfite content (curve 10) relative to the total SO_2 concentration. The relative content of SO_2 hydrate, sulfite, and pyrosulfite ions, as well as free MEA, does not exceed 0.7%.

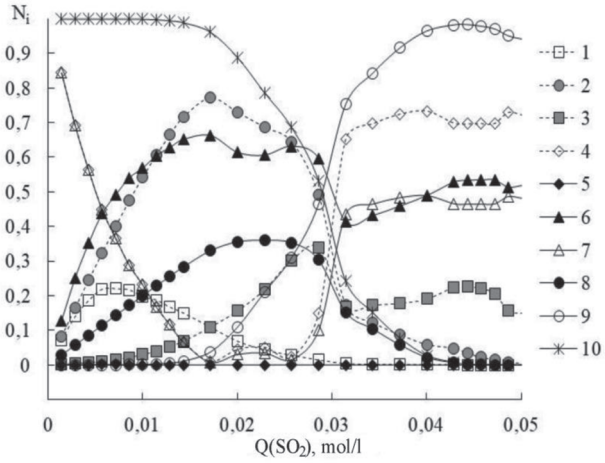

Fig. 11. Partial distribution diagrams of different forms of interaction in the SO_2 – MEA·1/3CA – H_2O system depending on Q_{SO_2} at 293 K. N_i – molar fraction of Cit^{3-} (1), $HCit^{2-}$ (2), H_2Cit^- (3), $C_{IIa} + C_{IIb} + C_{IIIa}$. (4, 7), $NH_2CH_2CH_2OH$ (5), $\overset{+}{N}H_3CH_2CH_2OH$ (6), C_{IS} (8, 10), HSO_3^-(9) relative to the total content of citrates (1–4), nitrogen (5–8) and sulfur (9, 10).

The concentration constants for the formation of ionic associates (β_{IIIS}, $\beta_{Ia} - \beta_{IIIa}$, $\beta_{Ib,}$ and β_{IIb}) have been calculated. Under the experimental conditions, these formation constants exceed 10.

The concentration and thermodynamic constants (β_{IIIS}) for ammonium sulfite formation in SO_2–MEA·1/3CA–H_2O solutions are nearly identical to those in SO_2 – MEA solutions [3, 20]. The dependences of $p\beta_i$ (for compounds **Ib**, **IIa,** and **IIIa**) on ionic strength (μ, M) follow a linear relationship (equation 29), whereas the dependence of $p\beta_{IIb} = f(\mu)$ is more complex (equation 30). The parameters of these equations are provided in Table 4.

$$p\beta_i = A_i + B_i \cdot \mu \quad (29)$$

$$p\beta_{IIb} = A_i + B_i \cdot \mu^{0,5} + C_i \cdot \mu \quad (30)$$

By definition [21], the coefficients A_i in equations 29 and 30 represent the negative decimal logarithms of the conditional thermodynamic constants ($\beta_{Ia} - \beta_{IIIa}$). As temperature increases, bond rearrangements occur in ionic associates **IIa**, **IIIa,** and compound **Ib**, as indicated by the lack of a clear dependence of $p\beta^T_{IIIa}$= f(T). Additionally, compounds **IIa** and **Ib** exhibit increased stability, as reflected in the A_i values of equation 29 (Table 4).

Table 4.

The values of the coefficients A_i, B_i in equation (29) for compounds Ib, IIa, and IIIa, and A_i, B_i, C_i in equation (30) for associate IIb in SO_2 – MEA·1/3CA – H_2O solutions *

T, K	A_i	B_i	R^2	$Q(SO_2):Q_N$
		IIIa		
288	-12.53	28.5	0.9142	0.0715÷0.172
293	-16.16	41.93	0.9384	0.0715÷0.129
303	-9.078	16.76	0.9735	0.0572÷0.257
313	-15.10	38.30	0.9492	0.0572÷0.486
		IIa		
283	-5.55	9.18	0.9868	0.072÷0.143
293	-8.10	21.6	0.9690	0.286÷0.515
		Ib		
283	-17.44	69.80	0.9839	0.400÷0.515
288	-20.24	87.86	0.9653	0.343÷0.458
303	0.05	0	–	0.315
		IIb		
	A_i	B_i	C_i	R^2	$Q(SO_2):Q_N$
283	-21.11	115.72	-191.1	0.9900	0.172÷0.372
288	-13.28	63.59	-88.61	0.9993	0.200÷0.315
293	-9.083	0	23.97	0.7959	0.172÷0.257
303	-1.730	0	0	–	0.286

*R^2 is the value of the approximation reliability.

With rising temperature, the absolute $p\beta^{T}_{IIb}$ values decrease, following a relationship described by equation 31 within the 283–303 K range.

$$p\beta^{T}_{IIb} = 264{,}15 - 88312/T, \quad (31)$$

where T is the absolute temperature, K.

Composition of SO_2 – MEA·1/6CA – H_2O solutions

For MEA·1/6CA solutions, in addition to reactions 1–24, there is also the potential formation of ion-molecular associates **IVa** and **IVb**, as described by equations 32 and 33.

$$3NH_2CH_2CH_2OH + 3\overset{+}{N}H_3CH_2CH_2OH + HOC_3H_4(COO^-)_3 \overset{\beta_{IVa}}{\rightleftarrows} \rightleftarrows \{NH_2CH_2CH_2OH\}_3\{\overset{+}{N}H_3CH_2CH_2OH\}_3\{HOC_3H_4(COO^-)_3\}, \quad (32)$$

$$2NH_2CH_2CH_2OH + 4\overset{+}{N}H_3CH_2CH_2OH + HOC_3H_4(COO^-)_3 \overset{\beta_{IVb}}{\rightleftarrows} \rightleftarrows \{NH_2CH_2CH_2OH\}_2\{\overset{+}{N}H_3CH_2CH_2OH\}_4\{HOC_3H_4(COO^-)_3\}. \quad (33)$$

Based on experimental data (Fig. 3a) and a mathematical model that incorporates the law of mass action (equations 1–18, 32, 33), along with the material balance equations for nitrogen (34), citrates (35), and sulfur (27), as well as the electroneutrality condition (36), the ionic-molecular composition of SO_2–MEA·1/6CA–H_2O solutions was determined (for example, Fig. 12).

$$Q_N = [NH_2CH_2CH_2OH] + [\overset{+}{N}H_3CH_2CH_2OH] + C_{Ia} + C_{Ib} + 2C_{IIa} + 2C_{IIb} + 3C_{IIIa} + 2C_{IS} + C_{IIS} + 2C_{IIIS} + 6C_{IVa} + 6C_{IVb} \quad (34)$$

$$Q_{Cit} = [HOC_3H_4(COOH)_3] + [HOC_3H_4(COOH)_2COO^-] + [HOC_3H_4(COOH)(COO^-)_2] + [HOC_3H_4(COO^-)_3] + C_{Ia} + C_{Ib} + C_{IIa} + C_{IIb} + C_{IIIa} + C_{IVa} + C_{IVb} \quad (35)$$

$$[H^+] + [\overset{+}{N}H_3CH_2CH_2OH] + C_{Ib} + C_{IIb} + C_{IVb} = [OH^-] + [HSO_3^-] + 2[S_2O_5^{2-}] + 2\cdot[SO_3^{2-}] \quad (36)$$

де $C_{IVa} = \{NH_2CH_2CH_2OH\}_3\{\overset{+}{N}H_3CH_2CH_2OH\}_3\{HOC_3H_4(COO^-)_3\}$,
$C_{IVb} = \{NH_2CH_2CH_2OH\}_2\{\overset{+}{N}H_3CH_2CH_2OH\}_4\{HOC_3H_4(COO^-)_3\}$.

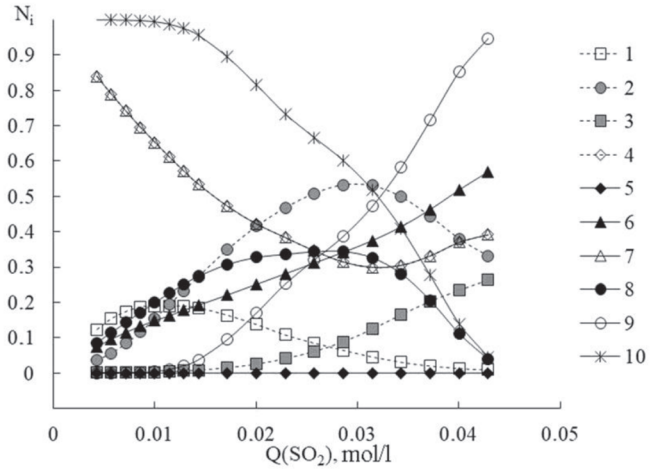

Fig. 12. Partial distribution diagrams of different forms of interaction in the SO_2–MEA·1/6CA–H_2O system depending on Q_{SO_2} at 293 K. Ni – molar fraction of Cit^{3-} (1), $HCit^{2-}$ (2), H_2Cit^- (3), C_{IVa}– (4, 7), $NH_2CH_2CH_2OH$ (5), $\overset{+}{N}H_3CH_2CH_2OH$ (6), C_{IS} (8, 10), HSO_3^- (9) relative to the total content of citrates (1–4), nitrogen (5–8) and sulfur (9, 10).

According to the calculations (Fig. 12), the chemisorption of sulfur dioxide by an MEA·1/6CA aqueous solution occurs due to its binding to monoethanolammonium sulfite **IS** (curve 10) at $Q(SO_2) < 0.0572$ mol/L, following reaction 37. This process is accompanied by:

$$2\{NH_2CH_2CH_2OH\}_3\{\overset{+}{N}H_3CH_2CH_2OH\}_3\{HOC_3H_4(COO^-)_3\} + 3SO_2\cdot H_2O \rightarrow 3(NH_3CH_2CH_2OH)_2SO_3 + 2HOC_3H_4(COO^-)_3 + 6\overset{+}{N}H_3CH_2CH_2OH \quad (37)$$

With further SO_2 addition, the relative content of hydrosulfite anions (curve 9) and monoethanolammonium cations (curve 6) increases due to reaction 38.

$$(NH_3CH_2CH_2OH)_2SO_3 + SO_2\cdot H_2O \rightarrow 2\overset{+}{N}H_3CH_2CH_2OH + 2HSO_3^- \quad (38)$$

In this case:

The mole fraction of the **IS** compound relative to total nitogen (curve 8) reaches a maximum at $Q(SO_2):Q_N = 1.0:4.0$;

The mole fraction of citrate anions (curve 1) reaches a maximum at $Q(SO_2):Q_N = 1.0:10.0$, accompanied by partial protonation of citrate anions with the formation of $HOC_3H_4(COOH)(COO^-)_2$ (curve 2) and dihydrocitrate anions (curve 3).

The relative content of $HOC_3H_4(COOH)(COO^-)_2$ (curve 2) reaches a maximum at $Q(SO_2) = 0.0286$ mol/L, while $HOC_3H_4(COOH)_2COO^-$ (curve 3) increases throughout the studied range.

The content of unbound MEA (as a free base), undissociated CA, sulfite and pyrosulfite anions, and $SO_2\cdot H_2O$ does not exceed 0.02 relative units. Notably, ionic associates **IIa** and **IIb** are not formed during the chemisorption of SO_2 in the studied concentration ($Q(SO_2)$) and temperature ranges, unlike in the MEA·1/3CA solution.

The concentration dependences $\mu = f(Q(SO_2))$ exhibit complex behavior due to the multicomponent nature of the chemisorption system during SO_2 absorption (at 283–288 and 298–313 K). However, at 293 K, only the ion-molecular complex **IVa** is formed between MEA and CA, leading to a linear dependence:

$$\mu = 0{,}0177 + 1{,}0261\cdot Q(SO_2); \quad n = 14;\ R^2 = 0{,}9940. \quad (39)$$

Using the obtained component composition data for SO_2–MEA·1/6CA – H_2O solutions, the concentration constants for the formation of compounds **IIIS**, **Ia**, **Ib**, **IIIa**, **Iva**, and **IVb** were calculated. The dependence $p\beta_{IIb} = f(\mu)$ is described by equation 29, with parameters provided in Table 5.

With increasing temperature, bond weakening is observed in compounds **Ia**, **IIIa**, **IVa** and **IVb**, as indicated by an increase in $p\beta_i$ values, which are numerically equal to the A_i coefficients in equation 29 (Table 5). Conversely, the stability of complex **Ib** increases. The concentration and thermodynamic constants β_{IIIS} for SO_2–MEA·1/6CA–H_2O and SO_2–MEA·1/3CA–H_2O solutions show no significant difference compared to SO_2 – MEA solutions [3, 20].

Table 5.

The values of the A_i, B_i coefficients in equation (29) for compounds Ia, Ib, IIIa, IVa, and IVb in SO_2–MEA·1/6CA–H_2O in solutions*

T, K	A_i	B_i	R^2	$Q(SO_2):Q_N$
		Ia		
303	-5,44	79,27	0,9954	0,315÷0,458
313	19,11	-274,7	0,9890	0,286÷0,400
		Ib		
283	-3,94	6,63	0,9895	0,315÷0,949
288	-5,08	-9,78	0,9741	0,257÷0,486
		IIIa		
288	-17,33	-102,56	0,9978	0,0715÷0,200
313	-6,873	41,14	0,9995	0,0286÷0,143
		IVa		
293	-12,16	-45,31	0,9885	0,014÷0,529
313	22,835	-382	0,8303	0,172÷0,257
		IVb		
283	-18,14	15,30	0,9920	0,072÷0,286
303	18,23	-377,0	0,9935	0,175÷0,263

*R^2 – the value of the approximation confidence.

CONCLUSIONS.

This study, based on pH, redox, and conductometric analyses, evaluates the acid-base interaction during the chemisorption of sulfur dioxide by aqueous solutions of monoethanolammonium and polyethylenepolyammonium citrates in comparison with sodium citrate.

The composition and relative stability of the reaction products formed during SO_2 interaction with aqueous solutions of Na_3Cit, MEA·1/3CA, PEPA·1/3CA, MEA·1/6CA, and PEPA·1/6CA were determined. It was shown that in the presence of ammonium citrates (MEA and PEPA), the following species are formed: ionic associates **Ia, IIa, IIb, IIIa**; ion-molecular associates **Ib, IVa, IVb**; and ammonium sulfites, hydrosulfites, and pyrosulfites. The component composition, as well as the concentration and thermodynamic constants of these associates, were calculated. In SO_2–MEA·1/3CA–H_2O solutions, increasing temperature enhances the relative stability of compounds **IIa** and **Ib**. In SO_2–MEA·1/6CA–H_2O solutions, the stability of compounds **Ia, IIIa, IVa** and **IVb** decreases, while **Ib** increases with rising temperature. Adding CA to the SO_2–MEA–H_2O system in MEA:CA ratios of 3:1 and 6:1 has no significant effect on the concentration and thermodynamic constants of ammonium sulfites formation.

The results obtained will be applied in the development of chemosorbents for respiratory protection.

ACKNOWLEDGEMENT. The work was carried out within the framework of the state budget theme "Scientific principles of creating hybrid fibrous filter materials for personal and collective protection equipment", state registration number: 0124U000930.

СКЛАД ТА ВІДНОСНА СТІЙКІСТЬ ПРОДУКТІВ ВЗАЄМОДІЇ ДІОКСИДУ СІРКИ З ВОДНИМИ РОЗЧИНАМИ ЦИТРАТІВ МОНОЕТАНОЛАМОНІЮ ТА ПОЛІЕТИЛЕНПОЛІАМОНІЮ

Р. Є. Хома, К. В. Циганенко, Т. С. Бєньковська, Ю. В. Ішков, С. В. Водзінський

Одеський національний університет імені І. І. Мечникова,
вул. Дворянська, 2, Одеса 65082, Україна
email: rek@onu.edu.ua

В роботі наведено результати pH-, редокс- та кондуктометричного дослідження кислотно-основної взаємодії при хемосорбції діоксиду сірки водними розчинами на основі 0,1 моль/л цитратів моноетаноламонію (МЕА·1/3СА) та поліетиленполіамонію (РЕРА·1/3СА), а також буферними розчинами моноетаноламін – цитрат моноетаноламонію (МЕА·1/6СА) та поліетиленполіамін – цитрат поліетиленполіамонію (РЕРА·1/6СА) у порівнянні із цитратом натрію. Встановлено склад сполук, що утворюються при поглинанні SO_2 розчинами Na_3Cit, МЕА·1/3СА, РЕРА·1/3СА, МЕА·1/6СА, РЕРА·1/6СА при 273 – 313 К. За одних і тих самих значень кількості поглинутого діоксиду сірки) для розчинів SO_2–Na_3Cit–H_2O та SO_2–МЕА·1/3СА–H_2O відмічено збільшення значень питомої електропровідності (æ) з ростом температури при 273–313 К; значення Δæ зменшуються в системах SO_2–МЕА·1/3СА–H_2O, SO_2–РЕРА·1/3СА–H_2O, SO_2–МЕА·1/6СА–H_2O та SO_2–РЕРА·1/6СА–H_2O під час нагрівання при 283–303 К, що спричинено їхнім йон-молекулярним складом. На основі розроблених математичних моделей розраховано йон-молекулярний компонентний склад розчинів SO_2– МЕА·1/3СА–H_2O та SO_2–МЕА·1/6СА–H_2O при 283–313 К та концентраційні і термодинамічні константи утворення іонних асоціатів: $(NH_3CH_2CH_2OH)_2SO_3$, $\{\overset{+}{N}H_3CH_2CH_2OH\}\{HOC_3H_4(COOH)_2(COO^-)\}$ (**Ia**), $\{\overset{+}{N}H_3CH_2CH_2OH\}_2\{HOC_3H_4(COOH)(COO^-)_2\}$ (**IIa**), $\{\overset{+}{N}H_3CH_2CH_2OH\}_2\{HOC_3H_4(COOH)_2(COO^-)\}$ (**IIb**), $\{\overset{+}{N}H_3CH_2CH_2OH\}_3\{HOC_3H_4(COO^-)_3\}$ (**IIIa**), а також іон-молекулярних асоціатів $\{\overset{+}{N}H_3CH_2CH_2OH\}\{HOC_3H_4(COOH)_3\}$ (**Ib**), $\{NH_2CH_2CH_2OH\}_3\{\overset{+}{N}H_3CH_2CH_2OH\}_3\{HOC_3H_4(COO^-)_3\}$ (**IVa**), $\{NH_2CH_2CH_2OH\}_2\{\overset{+}{N}H_3CH_2CH_2OH\}_4\{HOC_3H_4(COO^-)_3\}$ (**IVb**).

У розчинах SO_2–МЕА·1/3СА–H_2O з ростом температури відбувається перегрупування зв'язків у іонних асоціатах **IIa** та **Ib**, на що вказує відсутність чіткої температурної залежності $p\beta^T_{IIIa}$, а також зміцнення сполук **IIa** та **Ib**. В розчинах SO_2–МЕА·1/6СА–H_2O з підвищенням температури відбувається послаблення зв'язків у сполуках **Ia**, **IIIa**, **IVa** та **IVb**, а у сполуці **Ib**, навпаки, посилення.

Ключові слова: діоксид сірки, амонієві цитрати, кислотно-основна взаємодія, іонні асоціати, іон-молекулярні асоціати.

REFERENCES

1. Hanif M.A., Ibrahim N., Abdul Jalil A. Sulfur dioxide removal: An overview of regenerative flue gas desulfurization and factors affecting desulfurization capacity and sorbent regeneration. *Environ. Sci. Pollut. Res.* 2020. **27**: 27515–27540.
doi: 10.1007/s11356-020-09191-4
2. Hou Y., Chen Y., He X., Wang F., Cai Q., Shen B. Insights into the adsorption of CO_2, SO_2 and NO_x in flue gas by carbon materials: A critical review. *Chem. Eng. J.* 2024. **490**: 151424.
doi: 10.1016/j.cej.2024.151424
3. Khoma R.E. Acid-base interaction and sulfooxidation at chemosorption of sulfur dioxide by alkylamines aqueous solutions. Abstract of Doctor's degree dissertation, 02.00.01. Kyiv, 2019, 50 p. (*in Ukrainian*).
4. Khoma R.E., Bienkovska T.S., Gelmboldt V.O., Klimov D.G., Horlichenko M.G. Composition and the relative stability of sulfur dioxide interaction products with potassium and monoethanolammonium taurates aqueous solutions. Prolonged-action chemosorbent. *Visn. Odes. nac. univ., Him.* 2023: **28**(3): 35–51.
doi: 10.18524/2304-0947.2023.3(86).297810.
(*in Ukrainian*).
5. Ennan A. A.-A., Khoma R.E., Dlubovskii R.M., Zukharenko Yu.S., Benkovska T.S., Knysh I.M. Mono- and bifunctional impregnated fiber chemosorbents for respiratory purpose. *Visn. Odes. nac. univ., Him.* 2022. **27**(1): 6–36.
doi: 10.18524/2304-0947.2021.4(80).248297.
(*in Ukrainian*).
6. Bekassy-Molnar E., Marki E., Majeed J.G. Sulphur dioxide absorption in air-lift-tube absorbers by sodium citrate buffer solution. *Chem. Eng. Process*. 2005. **44**(9): 1039–1046.
DOI: 10.1016/j.cep.2005.02.001
7. Jiang X., Liu Y., Gu M. Absorption of Sulfur Dioxide with Sodium Citrate Buffer Solution in a Rotating Packed Bed. *Chin. J. Chem. Eng.* 2011: **19**(4): 687–692.
doi: 10.1016/s1004-9541(11)60042-6
8. Sun Z., Zhou Y., Jia S., Wang Y., Jiang D., Zhang L. Enhanced SO_2 Absorption Capacity of Sodium Citrate Using Sodium Humate. *Catalysts*. 2021: **11**(7): 865.
doi: 10.3390/catal11070865
9. Khoma R.E., Bienkovska T.S., Tsyganenko K.V., Karych A.M., Kononchenko A.R. Acid-base and electrochemical behavior of monoethanolamine (polyethylenepolyamine) – citric acid – water solutions. *J. Chem. Technol.* 2024: **32**(1): 30–42.
doi: 10.15421/jchemtech.v32i1.292412.
(*in Ukrainian*).
10. Khoma R.E., Bienkovska T.S. Water vapor, sulfur dioxide and ammonia adsorption by fibrous material impregnated with citrate-monoethanolamine buffer solutions. *Visn. Odes. nac. univ. Him*. 2024: **29**(2):101–116.
doi: 10.18524/2304-0947.2024.2(88).322135.
(*in Ukrainian*).
11. Apelblat A. Citric acid. *Springer*. 2014. 357 p.
doi: 10.1007/978-3-319-11233-6
12. Verhoff F.H., Bauweleers H. Citric acid. in Ullmann's Encyclopedia Ind. Chem. 2014. 11 p.
doi: 10.1002/14356007.a07_103.pub3
13. Citric acid. Available at https://pubchem.ncbi.nlm.nih.gov/compound/Citric-Acid#section=Solubility
14. Apelblat A., Manzurola E. Extraction of Citric Acid by n-Octanol and n-Hexanol. Ber. *Bunsenges Phys. Chem.* 1988. **92**(7): 793–796.
doi: 10.1002/bbpc.198800195
15. *Sodium citrate*. EHS Support. 2021. 8 p. Available at https://www.santos.com/wp-content/uploads/2021/04/Sodium-citrate-March-2021.pdf

16. *Sodium Citrate, Dihydrate*. LabChem. Safety Data Sheet. 2020. 6 p. Available at https://ehslegacy.unr.edu/msdsfiles/36924.pdf
17. *Monoethanolamine*. Available at https://pubchem.ncbi.nlm.nih.gov/compound/Monoethanolamine#section=Carcinogen-Classification
18. *Polyamine B*. SDS AkzoNobel. 2014. 125 p. Available at https://www.alliancechemicals.com/wp-content/uploads/2011/10/Polyamine BSDS.pdf
19. *Polyethylene Polyamine*. Chem BK. Available at https://www.chembk.com/en/chem/Polyethylene%20Polyamine
20. Khoma R.E., Shestaka A.A., Gelmboldt V.O. On interaction of sulfur(IV) oxide with aqueous solutions of ethanolamines. *Russ. J. Appl. Chem.* 2012: **85**(11):1667–1675. doi: 10.1134/S1070427212110067
21. Hartley F.R., Burgess C., Alcock R.M. Solution Equilibria. Ellis Horwood Limited: Chichester, West Sussex, England. 1980. 361 p.

Стаття надійшла 05.01.2025.

УДК 547.7/.8 doi: 10.33609/2708-129X.91.3.2025.25-33

ЕФЕКТИВНИЙ СПОСІБ УТВОРЕННЯ 2-СТИРИЛПІРИМІДИН-4(3Н)-ОНІВ

А. О. Яволовський[1], Л. В. Грищук[1], С. М. Плужник-Гладир[1], А. С. Давтян[1], Д. Е. Степанов[1], Ю. В. Ішков[2], Г. Л. Камалов[1]

[1]Фізико-хімічний інститут ім. О. В. Богатського Національної академії наук України, Люстдорфська дорога, 86, Одеса 65080,Україна;
[2]Одеський Національний університет імені І. І. Мечникова МОН України, вул. Дворянська, 2, Одеса 65082, Україна,
e-mail: sergey_pluzhnik@ukr.net

Розроблено зручну схему синтезу сполук ряду (*E*)-6-R-2-стирилпіримідин-(4*H*)-онів відновленням 2-(2-оксо-2-арилетиліден)-2,3-дигідропіримідин-4(1*H*)-онів боргідридом натрію з подальшою дегідратацією отриманих 2-(2-гідрокси-2-арилетил) піримідин-4(3*H*)-онів у ортофосфорній кислоті за підвищеної температури. Запропоновано два варіанти модифікації 2-стирилпіримідин-4(3*H*)-онів. А саме: синтезовані 4-метилбензосульфонати, а також встановлено, що за взаємодії (*E*)-6-метил-2-стирилпіримідин-(4*H*)-ону з еквімолекулярною кількістю Br_2, продуктом реакції виявився (*E*)-5-бром-6-R-2-стирилпіримідин-(4*H*)-он. Будову синтезованих сполук встановлено за допомогою ЯМР-спектроскопії і мас-спектрометрії.

Ключові слова: 2-(2-оксо-2-арилетилсульфаніл)-піримідин-4(*3H*)-они, 2-(2-гідрокси-2-арилетил)піримідин-4(3*H*)-они, (*E*)-6-R-2-стирилпіримідин-(4*H*)-они, відновлення, дегідратація, бромування, синтез, будова.

ВСТУП. Серед штучних фоточутливих систем помітне місце займають похідні стильбену. Вони є синтетично доступними сполуками, які виявляють здатність до молекулярного фотоперемикання з високою ефективністю і характеризуються мультифотохромними властивостями [1–3]. Несиметричні гетариларилетени (у тому числі ізомерні стирилпіримідини) є менш дослідженими, ніж симетричні похідні. На сьогодні відомо декілька методів синтезу 2-стирилпіримідинів. Перші два полягають в утворенні піримідинового циклу шляхом конденсації естеру імінокоричної кислоти з естером 3-амінокротонової кислоти [4] або естеру коричної кислоти з амідом 3-амінокротонової кислоти [5]. Виходи 6-метил-2-стирилпіримідин-4(3*H*)-ону становлять, відповідно, 22% і 33%. Відомі також методи отримання низки 2-стирилпіримідинів конденсацією 2-метилпіримідинів із бензальдегідами; виходи кінцевих

продуктів суттєво залежать від кислотності метальної групи вихідних піримідинів та каталізатора [6,7].

Роботу присвячено розробленню альтернативного варіанту синтезу 2-стирилпіримідинів шляхом послідовного відновлення та дегідратації 2-(2-оксо-2-арилетиліден)-2,3-дигідро-1*H*-піримідин-4-онів. Запропоновані методики синтезу і виділення дозволяють отримати цільові продукти з високими виходами і достатнім ступенем чистоти без додаткового очищення проміжних спиртів та з мінімальним використанням органічних розчинників.

ЕКСПЕРИМЕНТ І ОБГОВОРЕННЯ РЕЗУЛЬТАТІВ. Відновлення карбонільної групи вихідних 2-(2-оксо-2-арилетиліден)-2,3-дигідропіримідин-4(1*H*)-онів **1a-d** [8, 9] здійснювали надлишком боргідриду натрію у етанолі (рис 1).

Використана методика синтезу і виділення 2-(β-гідроксиалкіл)-піримідин-4(*3H*)-онів (**2a-d**) дозволила отримати продукти з високими виходами і достатнім ступенем чистоти без додаткового очищення. Дегідратацію спиртів з утворенням подвійного C=C-зв'язку можна здійснювати як каталітичними методами, так і дією речовин, що від'єднують воду. Найважливішими речовинами, які використовують у препаративній хімії для цих цілей, є мінеральні та органічні кислоти, ангідриди борної і фосфорної кислоти, йод, ацетилхлорид. Оскільки у нашому випадку спирти є твердими речовинами, то як дегідратуючий засіб ми використали ортофосфорну кислоту, яка водночас виконувала роль розчинника. Реакцію здійснювали в інтервалі температур 150–200 °C (рис 1).

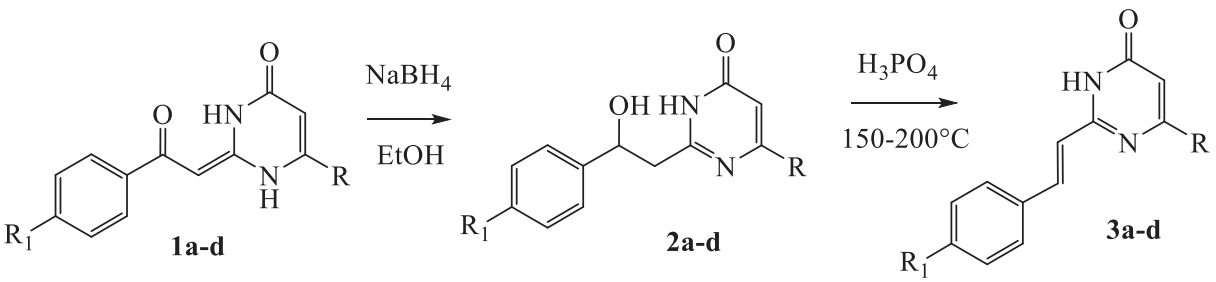

R=Me, R_1=H (**a**); R=Me, R_1=Ph (**b**); R=Ph, R_1=H (**c**); R=R_1=Ph (**d**)

Рис. 1. Загальна схема синтезу (*E*)-6-R-2-стирилпіримідин-(4*H*)-онів **3a-d**
Fig. 1. General scheme for the synthesis of (E)-6-R-2 styrylpyrimidin-(4H)-ones **3a-d**.

За даними ЯМР ^{1}H, сполуки **3a-d** існують у формі трансізомерів.

На прикладі речовин **3a, e** (рис. 2) було досліджено можливість використання сульфонатного методу як першої стадії модифікації зазначеного вище класу сполук. Реакцію проводили з надлишком *n*-толуолсульфохлориду в тетрагідрофурані за кімнатної температури. Як основу використовували триетиламін.

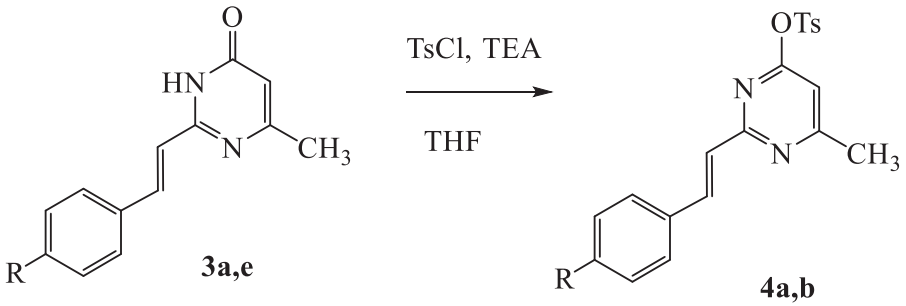

R=H (**a**); R=NO_2 (**e, b**)

Рис. 2. Схема утворення сульфонатів
Fig. 2. Scheme of sulfonate formation.

Виходи кінцевих продуктів – середні. Суттєвим недоліком цієї методики можна вважати дуже повільний перебіг реакції – близько 30 діб.

Однією з характерних властивостей алкенів є утворення 1,2-дигалогеналканів. Реакція протікає за іонним механізмом типу електрофільного приєднання. У нашому випадку при взаємодії (*E*)-6-метил-2-стирилпіримідин-4(3*H*)-ону (**3a**) з еквімолярною кількістю брому було виділено не очікуваний продукт приєднання **5** (рис. 3), а продукт заміщення атома водню у положенні «5» гетероциклу **6** (рис. 3).

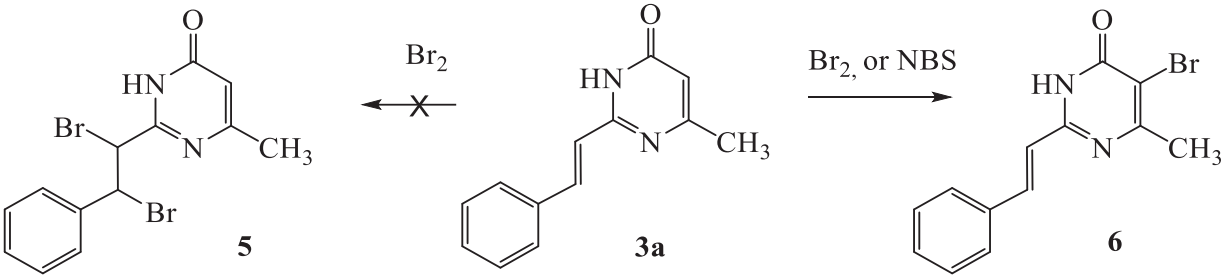

Рис. 3. Схема бромування сполуки **3a**
Fig. 3. Scheme of bromination of a compound **3a**.

Подібний напрям реакції можна пояснити утворенням на першій стадії реакції активного інтермедіату, а саме N-бромпіримідину. Опосередковано на користь цього припущення свідчить факт утворення сполуки **6** при бромуванні **3a** N-бромсукцинімідом.

Контроль за ходом реакції і чистотою синтезованих речовин здійснювали методом ТШХ на пластинах Silufol UV-254-VIS, елюент хлороформ-ацетонітрил-гексан, 5:2:1, та метанол-ацетонітрил-хлороформ, 1:2:5. Мас-спектри (FAB) отримано на мас-спектрометрі VG Analitical 7070 ED.

Спектри ЯМР ^{1}H і ^{13}C отримано на спектрометрі Varian WXP-500 (робоча частота 499.88 і 125.71 МГц відповідно), внутрішній стандарт – $SiMe_4$.

2-(2-Гідрокси-2-фенілетил)-6-метилпіримідин-4(3Н)-он (**2a**) 1 г (4 ммоль) речовини **1a** і 0.1 г $NaBH_4$ у 100 см^3 етанолу перемішували протягом 5 діб магнітною мішалкою, додаючи на другу і третю добу ще дві порції $NaBH_4$ по 0.1 г Після закінчення реакції (контроль методом ТШХ, елюент – хлороформ-ацетонітрил-гексан, 5:2:1) реакційну суміш нейтралізували HCl, перемішуючи, і фільтрували осад. Фільтрат випарювали на роторному випарнику насухо. Твердий залишок промивали водою і фільтрували на фільтрі Шотта. Вихід 0.9 г (89%), безбарвні кристали, т. топл. = 155–160 °С. Спектр ЯМР ^{1}H (DMSO-d^6), δ, м.ч.: 2.14 с (3Н CH_3), 2.80 д (2Н, CH_2, *J* 5.8 Гц), 5.04–5.10 м (1Н, СН), 5.55 розш. с (1Н, ОН), 6.02 с (1Н, $CH_{піримідин}$), 7.22 т (1Н, $CH_{аром}$, *J* 7.6 Гц), 7.31 т (2Н, 2$CH_{аром}$, *J* 7.6 Гц), 7.37 д (2Н, 2$CH_{аром}$, *J* 7.6 Гц), 12.22 с (1Н, NH). Спектр ЯМР ^{13}C (DMSO-d^6): 23.40, 44.35, 70.80, 110.03, 125.68, 127.09, 128.12, 144.80, 159.53, 162.40, 164.31. Мас-спектр: 231 $[M+H]^+$. Знайдено, %: С 67.70, Н 6.20, N 12.09. $C_{13}H_{14}N_2O_2$. Розраховано, %: С 67.81, Н 6.13, N 12.14.

2-(2-([1,1`-біфеніл]-4-іл)-гідроксиетил)-6-метилпіримідин-4(3Н)-он. (**2b**). Отримували аналогічно з речовини **1b**. Вихід 80%, безбарвні кристали, т. топл. = 210–215°С. Спектр ЯМР ^{1}H (DMSO-d^6), δ, м.ч.: 2.16 с (3Н CH_3), 2.85 д (2Н, CH_2, *J* 8.8 Гц), 5.12–5.16 м (1Н, СН), 5.55 розш. с (1Н, ОН), 6.03 с (1Н, $CH_{піримідин}$), 7.33 т (1Н, $CH_{аром}$, *J* 7.6 Гц), 7.42 т (2Н, 2$CH_{аром}$, *J* 7.6 Гц), 7.47 д (2Н, 2$CH_{аром}$, *J* 7.6 Гц), 7.62 д (2Н, 2$CH_{аром}$, *J* 7.6 Гц), 7.64 д (2Н, 2$CH_{аром}$, *J* 7.6 Гц), 12.22 розш. с (1Н, NH). Спектр ЯМР ^{13}C (DMSO-d^6): 164.22, 162.52, 159.55, 144.08, 140.00, 139.01, 128.91, 127.32, 126.59, 126.46, 126.33, 110.04, 70.54, 44.29, 23.30. Мас-спектр: 307 $[M+H]^+$. Знайдено, %: С 79.50, Н 6.00, N 9.00. $C_{19}H_{18}N_2O_2$. Розраховано, %: С 79.49, Н 5.92, N 9.14.

2-(2-Гідрокси-2-фенілетил)-6-фенілпіримідин-4(3Н)-он (**2c**). Отримували аналогічно з речовини **1c.** Вихід 90%, безбарвні кристали, т. топл. = 210–220°С. Спектр ЯМР ^{1}H (DMSO-d^6), δ, м.ч.: 2.96 д (2Н, CH_2, *J* 6.8 Гц), 5.21 дд (1Н, СН, *J* 11.0, 6.8 Гц), 5.61 д (1Н, ОН, *J* 4.5 Гц), 6.74 с (1Н, $CH_{піримідин}$), 7.25 т (1Н, $CH_{аром}$, *J* 7.3 Гц), 7.34 т (2Н, 2$CH_{аром}$, *J* 7.3 Гц), 7.43 д (2Н, 2$CH_{аром}$, *J* 7.3 Гц), 7.47–7.49 м (3Н, 3$CH_{аром}$), 8.04–8.06 м (2Н, 2$CH_{аром}$), 12.45 с (1Н, NH). Спектр ЯМР ^{13}C (DMSO-d^6): 45.11, 71.33, 107.48, 126.28, 127.40, 127.55, 128.60, 129.11, 130.83, 136.85, 145.33, 160.50, 161.02, 163.37. Мас-спектр: 293 $[M+H]^+$. Знайдено, %: С 74.00, Н 5.60, N 9.50. $C_{18}H_{16}N_2O_2$. Розраховано, %: С 73.95, Н 5.52, N 9.58.

2-(2-([1,1`-біфеніл]-4-іл)-гідроксиетил)-6-фенілпіримідин-4(3Н)-он (**2d**). Отримували аналогічно з речовини **1d**. Вихід 75%, безбарвні кристали, т. топл. = 260–262°С. Спектр ЯМР ^{1}H (DMSO-d^6), δ, м.ч.: 2.98 д (2Н, CH_2, *J* 5.6 Гц), 5.23–5.26 м (1Н, СН), 5.62 розш. с (1Н, ОН), 6.73 с (1Н, $CH_{піримідин}$), 7.33 т (1Н, $CH_{аром}$, *J* 7.3 Гц), 7.42–7.50 м (7Н, 7$CH_{аром}$), 7.62–7.64 м (4Н, 4$CH_{аром}$), 8.02–8.06 м (2Н, 2$CH_{аром}$), 12.44 розш. с (1Н, NH). Спектр ЯМР ^{13}C (DMSO-d^6): 162.92, 160.58, 159.96, 144.05, 140.00, 139.01, 136.39, 130.35, 128.91, 128.63, 127.32, 126.94, 126.59, 126.45, 126.43, 107.04, 70.59, 44.55. Мас-спектр: 369 $[M+H]^+$. Знайдено, %: С 78.20, Н 5.50,

N 7.50. $C_{24}H_{20}N_2O_2$. Розраховано, %: C 78.24, H 5.47, N 7.60.

(E)-6-Метил-2-стирилпіримідин-4(3H)-он (**3a**). 0.23 г (6 ммоль) речовини **2a** у 7 см^3 ортофосфорної кислоти витримували протягом 0.5 год. за температури 150–200 °C. Після охолодження реакційну суміш перемішували з 100 см^3 води і фільтрували на фільтрі Шотта. Осад промивали водою до нейтральної реакції фільтрату, сушили на повітрі. Вихід 0.18 г (85%), безбарвні кристали, т. топл. = 223–225°C. Спектр ЯМР ^{1}H (DMSO-d^6), δ, м.ч.: 2.19 с (3H CH_3), 6.05 с (1H, $CH_{піримідин}$), 6.88 д (1H, $CH_{алкен,}$ *J* 16.1 Гц) 7.37–7.59 м (3H, $CH_{аром}$), 7.59 д (2H, 2$CH_{аром}$, *J* 7.8 Гц), 7.83 д (1H, $CH_{алкен,}$ *J* 16.1 Гц) 9.76 с (1H, NH). Спектр ЯМР ^{13}C (DMSO-d^6): 23.41, 110.23, 120.29, 127.69, 129.04, 129.90, 134.75, 138.99, 155.38, 162.59, 164.19. Мас-спектр: 213 $[M+H]^+$. Знайдено, %: 73.52, H 5.73, N 13.17. $C_{13}H_{12}N_2O$. Розраховано, %: C 73.56, H 5.70, N 13.20.

(E)-2-(2-([1,1`-біфеніл]-4-іл)вініл)-6-метилпіримідин-4(3H)-он. (**3b**). Отримували аналогічно з речовини **2b**. Вихід 98%, безбарвні кристали, т. топл. > 250°C розкл. Спектр ЯМР ^{1}H (DMSO-d^6), δ, м.ч.: 2.21 с (3H CH_3), 6.06 с (1H, $CH_{піримідин}$), 6.90 д (1H, $CH_{алкен,}$ *J* 16.1 Гц) 7.32–7.71 м (9H, $CH_{аром}$), 7.89 д (1H, $CH_{алкен,}$ *J* 16.1 Гц) 10.07 с (1H, NH). Спектр ЯМР ^{13}C (DMSO-d^6): 164.99, 162.80, 155.83, 141.83, 139.67, 138.74, 134.34, 129.46, 128.71, 128.35, 127.67, 127.08, 120.73, 110.60, 24.02. Мас-спектр: 289 $[M+H]^+$. Знайдено, %: C 79.10, H 5.60, N 9.70. $C_{19}H_{16}N_2O$. Розраховано, %: C 79.14, H 5.59, N 9.72.

(E)-6-Феніл-2-стирилпіримідин-(4H)-он (**3c**). Отримували аналогічно з речовини **2c**. Вихід 93%, безбарвні кристали, т. топл. = 270–272°C. Спектр ЯМР ^{1}H (DMSO-d^6), δ, м.ч.: 6.79 с (1H, $CH_{піримідин}$), 7.02 д (1H, $CH_{алкен,}$ *J* 16.0 Гц), 7.43-7.54 м (6H, $CH_{аром}$), 7.68 д (2H, $CH_{аром}$, *J* 7.5 Гц), 8.05 д (1H, $CH_{алкен,}$ *J* 16.1 Гц), 8.17 д (2H, $CH_{аром}$, *J* 7.5 Гц), 12.57 с (1H, NH). Спектр ЯМР ^{13}C (DMSO-d^6): 107.56, 121.09, 127.47, 128.28, 129.16, 129.57, 130.46, 130.95, 135.32, 136. 81, 139.90, 156.33, 161.13, 163.43. Мас-спектр: 275 $[M+H]^+$. Знайдено, %: C 78.80, H 5.15, N 10.20. $C_{18}H_{14}N_2O$. Розраховано, %: C 78.81, H 5.14, N 10.21.

(E)-2-(2-([1,1`-біфеніл]-4-іл)вініл)-6-фенілпіримідин-4(3H)-он (**3d**)

Отримували аналогічно з речовини **2d**. Вихід 99%, безбарвні кристали, т. топл. >290 °C розкл. Мас-спектр: 351 $[M+H]^+$. Знайдено, %: C 82.23, H 5.20, N 7.97. $C_{24}H_{18}N_2O$. Розраховано, %: C 82.26, H 5.18, N 7.99.

6-Метил-2-стирилпіримідин-4-іл 4-метилбензосульфонат (**4a**)

До суміші 0.6 г (3 ммоль) сполуки **3a** і 0.8 г (4 ммоль) *n*-толуолсульфохлориду в 60 см^3 безводного ТГФ додавали 0.6 см^3 перегнаного триетиламіну і залишали на 30 діб в ізольованій ємкості за кімнатної температури. Гідрохлорид триетиламіну, що виділився з реакційної суміші, відфільтровували. Фільтрат випарювали на роторному випарнику. Решту промивали водою і фільтрували через фільтр Шотта, сушили під зниженим тиском водоструминного насоса. Потім проводили екстракцію горячим гептаном. Осад, що виділився при охолодженні екстракту, відділяли фільтрацією. Вихід 0.5 г (58%), безбарвні кристали, т. топл. = 153–157°C. Спектр ЯМР ^{1}H ($CDCl_3$), δ, м.ч.: 2.44 с (3H, CH_3), 2.50 с (3H, CH_3), 6.73 с (1H, $CH_{піримідин}$), 7.33 д (1H, $CH_{аром}$ *J*.8.0 Гц), 7.03 д (1H, $CH_{алкен,}$ *J* 16.2 Гц), 7.37 т (2H, 2$CH_{аром}$, *J*.8.0 Гц), 7.52 д (2H, 2$CH_{аром}$,

J 7.8 Гц), 7.59 д (2Н, $2CH_{алкен}$, 16.2 Гц), 7.98 д (1Н, $CH_{аром,}$ *J*8.0 Гц). Спектр ЯМР ^{13}C ($CDCl_3$): 21.31, 23.57, 107.04, 125.75, 127.13, 128.38, 128.90, 129.22, 133.53, 135.21, 139.02, 145.18, 163.62, 164.29, 170.34. Мас-спектр: 367 $[M+1]^+$. Знайдено, %: С 65.53, Н 7.54, N7.61. $C_{20}H_{18}N_2O_3S$. Розраховано, %: С 65.57, Н 7.50, N7.65.

6-Метил-2-(4-нітростирил)піримідин-4-іл 4-метилбензосульфонат (**4b**)

Отримували аналогічно з речовини **3e**. Вихід (53%), безбарвні кристали, т. топл. = 182–185°С. Спектр ЯМР ^1H ($CDCl_3$), δ, м.д.: 2.46 с (3Н, CH_3), 2.54 с (3Н, CH_3), 6.80 с ($1H_{піримідин}$), 7.16 д ($1H_{олефін}$, *J*16.0 Гц), 7.39 д ($2H_{аром}$, *J*8.0 Гц), 7.66 д ($2H_{аром}$, *J*8.5 Гц), 7.76 д ($1H_{олефін}$, *J*16.0 Гц), 7.97 д ($2H_{аром}$, *J*8.0 Гц), 8.23 д ($2H_{аром}$, *J*8.5 Гц). Спектр ЯМР ^{13}C ($CDCl_3$): 21.40, 23.76, 107.88, 123.71, 127.66, 128.30, 129.34, 130.04, 133.37, 136.13, 141.49, 145.38, 147.43, 163.26, 163.72, 170.62. Мас-спектр: 412 $[M+1]^+$. Знайдено, %: С 60.91, Н 4.12, N 5.61. $C_{20}H_{17}N_3O_5S$. Розраховано, %: С 58.39, Н 4.16, N 10.21.

Бромування (Е)-6-метил-2-стирилпіримідин-4(3Н)-ону. Перший варіант

У колбу Ерленмейера (100 см^3) зі зворотнім повітряним холодильником, обгорнуту чорним папером, поміщали 0,442 г (2.08 ммоль) (*E*)-6-метил-2-стирилпіримідин-4(3*H*)-ону (**3a**) та 30 см^3 тетрахлориду карбону і перемішували отриману суспензію у магнітній мішалці. Окремо в мірну колбу ємністю 50 см^3 поміщали 0.512 г брому і додавали до мітки тетрахлорид карбону. Від отриманого розчину відбирали 32.42 см^3 (містить 0,332 г, 2.08 ммоль брому) рідини і додавали її до субстрату. Через 5 хвилин утворювався об'ємний осад. Реакційну суміш залишали на ніч за кімнатної температури (15°С). Далі осад відділяли фільтруванням і кристалізували з етанолу. Вихід (*E*)-5-бром-6-метил-2-стирилпіримідин-4(3*H*)-ону (**6**) 0,378 г, (62%), безбарвні кристали, т. топл. = 270–271°С. Спектр ЯМР ^1H (DMSO-d^6), δ, м.ч.: 2.37 с (3Н CH_3), 6.84 д (1Н, $CH_{алкен,}$ *J* 16.0 Гц) 7.30–7.50 м (3Н, $CH_{аром}$), 7.5–7.70 м (2Н, $2CH_{аром}$), 7.84 д (1Н, $CH_{алкен,}$ *J* 16.0 Гц) 12.83 с (1Н, NH). Спектр ЯМР ^{13}C (DMSO-d^6): 25.02, 109.71, 119.68, 128.07, 129.53, 130.17, 134.99, 140.06, 154.00, 158.82, 162.79. Мас-спектр: 292 $[M+H]^+$. Знайдено, %: 53.58, Н 3.80, N 9.60. $C_{13}H_{11}BrN_2O$. Розраховано, %: С 53.61, Н 3.78, N 9.62.

Другий варіант. Колбу Ерленмейера (100 см^3) обладнують дворогим Ч-подібним форштосом. До центрального отвору форштосу приєднують зворотній повітряний холодильник. Боковий отвір форштосу обладнують скляною пробкою з пропущеною крізь неї фторопластовим тонким шлангом, одна частина якого занурена у реакціонну суміш, а друга приєднана до мікродозатора. В реакційну колбу поміщали суміш 0,442 г (2.08 ммоль) (*E*)-6-метил-2-стирилпіримідин-4(3*H*)-ону (**3a**) в 30 см^3 тетрахлориду карбону. Перемішували отриману суспензію у магнітній мішалці та через верхній отвір холодильника освітлювали УФ-лампою з довжиною хвилі 365 нм. Окремо 0.512 г брому поміщали в мірну колбу, ємністю 50 см^3, і додавали до мітки тетрахлорид карбону. Від отриманого розчину відбирали 32.42 см^3 (містить 0,332 г, 2.08 ммоль брому) і поршневим мікродозатором додавали його до субстрату протягом 90 хвилин. Далі реакційну суміш нагрівали 4 години за 50°С. Після охолодження об'ємний осад кремового кольору

відділяли фільтруванням і кристалізували з етанолу. Вихід (*E*)-5-бром-6-метил-2-стирилпіримідин-4(3*H*)-ону (**6**) (64%).

Третій варіант. До суспензії 0,426 г (2.01 ммоль) (*E*)-6-метил-2-стирилпіримідин-4(3*H*)-ону (**3а**) в 50 см^2 тетрахлориду карбону додавали 0,375 г (2,1 ммоль) сухого N-бромсукциніміду і перемішували 60 хвилин без нагрівання. Після цього реакційну суміш освітлювали УФ-лампою з довжиною хвилі 365 нм протягом 60 хвилин. Потім реакційну суміш кип'ятили 30 хвилин і залишали на ніч. Об'ємний жовто-помаранчевий осад, що випав, фільтрували, промивали тричі водою по 50 см^3 і сушили на повітрі. Кристалізували з етанолу. Вихід (*E*)-5-бром-6-метил-2-стирилпіримідин-4(3*H*)-ону (**6**) (76%).

ВИСНОВКИ. Розроблена методика відновлення карбонільної групи 2-(2-оксо-2-арилетиліден)-2,3-дигідропіримідин-4(1*H*)-онів дозволяє отримати відповідні спирти достатнього ступеня чистоти без додаткового очищення та з високими виходами. Подальша дегідратація вищеозначених сполук становить конкурентоздатний спосіб утворення (*E*)-6-R-2-стирилпіримідин-(4*H*)-онів, який має низку переваг (доступні вихідні речовини, високі виходи кінцевих сполук, використання мінімуму органічних розчинників) перед тими, які застосовували раніше.

Роботу виконано в рамках проєкту НАН України «Ефективні способи утворення 2-стирилпіримідинів на основі 2-(2-гідрокси-2-арилетил)-2,3-піримідин-4(3H)-онів», № 0121U107518.

EFFECTIVE METHOD FOR PRODUCING 2-STYRYLPYRIMIDIN-4(3H)-ONES.

A. A. Yavolovskii[1], L. V. Grishchuk[1], S. M. Pluzhnik-Gladyr[1], A. S. Davtian[1], D. E. Stepanov[1], Yu. V. Ishkov[2], G. L. Kamalov[1]

A. V. Bogatsky Physico-Chemical Institute of National Academy of Science of Ukraine, 86 Lustdorfska doroga, 65080 Odessa, Ukraine; [2]Odesa I. I. Mechnikov National University, 2 Dvorianska vul., 65082 Odesa, Ukraine e-mail: sergey_pluzhnik@ukr.net

A convenient scheme for the synthesis of a series of compounds of (E)-6-R-2-styrylpyrimidin-(4H)-ones by reduction of 2-(2-oxo-2-arylethylidene)-2,3-dihydropyrimidin-4(1H)-ones with sodium borohydride was developedfollowed by dehydration of the obtained 2-(2-hydroxy-2-arylethyl)pyrimidin-4(3H)-ones in orthophosphoric acid at elevated temperature.Two variants of modification of 2-styrylpyrimidin-4(3H)-ones are proposed. Namely, 4-methylbenzosulfonates were synthesized, and it was also established that upon the interaction of (E)-6-methyl-2-styrylpyrimidin-(4H)-one with an equimolecular amount of Br_2, the reaction product turned out to be (E)-5-bromo-6-R-2-styrylpyrimidine-(4H)-one.The structure of the synthesized compounds was established using NMR spectroscopy and mass spectrometry.

Keywords: 2-(2-Oxo-2-arylethylsulfanyl)-pyrimidin-4(3H)-ones, 2-(2-hydroxy-2-arylethyl)pyrimidin-4(3H)-ones, (E)-6-R-2-styrylpyrimidine-(4H)-ones, reduction, dehydration, bromination, synthesis, structure.

ЛІТЕРАТУРА

1. Yang J.-S. Spectroscopic Correlations between Supermolecules and Molecules. Anatomy of the Ion-Modulated Electronic Properties of the Nitrogen Donor in Monoazacrown-Derived Intrinsic Fluoroionophores / J.-S. Yang, C.-Y. Hwang, C.-C. Hsieh, S.-Y. Chiou. // *J. Org. Chem*. 2004. 69. P. 719–726. doi: 10.1021/jo035462k
2. Saito H. Diastereoselective [2+2] Photocycloaddition of Stilbene to Chiral Fumarate. Direct versus Charge-Transfer Excitation / H. Saito, T. Mori, T. Wada, Y. Inoue. // *J. Am. Chem. Soc.* 2004. 126. P. 1900. doi: 10.1021/ja0370140
3. Thelakkat M. Low molecular weight and polymeric heterocyclics as electron transport/ hole-blocking materials in organic light-emitting diodes / M. Thelakkat, H.-W. Schmidt. // *Polym. Adv. Technol.* 1998. 9. P. 429–442. doi:10.1002/(SICI)1099-1581(199807)9:7<429::AID-PAT798>3.0.CO;2-E
4. Ried W. Reaktionen mit Imidsäureestern. VI. Umsetzung von Imidsäureestern mit β-Amino-crotonsäureester /W. Ried, P. Stock. //*Ann. Chem., Justus Liebigs.* 1966. 700. 1. P. 87–91. doi: 10.1002/jlac.19667000112
5. Kato T. Studies on Ketene and Its Derivatives. LVIII. Reaction of 3-Aminocrotonamide with α, β-Unsaturated Esters / T. Kato, H. Yamanaka, H. Fukumi, M. Nada. // *Yakugaku zasshi.* 1973. 93(11). P. 1437–1444. doi: 10.1248/yakushi1947.93.11_1437
6. Haroutounian S. A. 4'-Hydroxystyryldiazines: Synthesis and Fluorescence Properties / S. A. Haroutounian, J. A. Katzenellenboger. // *Tetrahedron*. 1995. 51. P. 1585–1598. doi: 10.1016/0040-4020(94)01050-A
7. Perkampus H.-H., Bluhm T. Zurphotochemie der styryldiazine: Darstellung der Edukte und Produkte/ H.-H. Perkampus, T. Bluhm. // *Tetrahedron*. 1972. 28. P. 2099–2110. doi: 10.1016/0040-4020(72)88017-7
8. Hurst D. T., Beautont C., Jones D. T. E., Kingsley D. A., Partridge J. D., Rutherford T.The Chemistry of Pyrimidinethiols. II. The Preparation and Reactions of Some 2-Arenecarbonylmethylthiopyrimidines. *J. Aust. J. Chem.* 1988. V. 41. P. 1209–1219. doi: 10.1071/CH9881209
9. Stepanov D.E., Grishuk L.V., Ivanov R.Yu., Yavolovskii A.A., Kamalov G.L. A simple approach to the synthesis of 2-(2-amino-4-arilthiazol-5-yl)pyrimidines. *Rus. J. Gen. Chem.* 2013. N **3** (83). P. 526–529. doi: 10.1134/S1070363213030195

REFERENCES

1. Yang J.-S. Spectroscopic Correlations between Supermolecules and Molecules. Anatomy of the Ion-Modulated Electronic Properties of the Nitrogen Donor in Monoazacrown-Derived Intrinsic Fluoroionophores. *J. Org. Chem*. 2004. **69**. 719–726. doi: 10.1021/jo035462k
2. Saito H., Mori T., Wada T., & Inoue Y. Diastereoselective [2+2] photocycloaddition of stilbene to chiral fumarate. Direct versus charge-transfer excitation. *Journal of the American Chemical Society*. 2004. **126**(6): 1900–1906. doi: 10.1021/ja0370140
3. Thelakkat M. Low molecular weight and polymeric heterocyclics as electron transport/ hole-blocking materials in organic light-emitting diodes. *Polym. Adv. Technol.* 1998. **9**. 429–442. doi:10.1002/(SICI)1099-1581(199807)9:7<429::AID-PAT798>3.0.CO;2-E
4. Ried W. Reaktionen mit Imidsäureestern, VI. Umsetzung von Imidsäureestern mit β-Amino-crotonsäureester. *Ann. Chem., Justus Liebigs.* 1966. **700**(1): 87–91. doi: 10.1002/jlac.19667000112
5. Kato T. Studies on Ketene and Its Derivatives. LVIII. Reaction of 3-Aminocrotonamide with

α, β-Unsaturated Esters. *Yakugaku zasshi.* 1973. **93**(11): 1437–1444.
doi: 10.1248/yakushi1947.93.11_1437

6. Haroutounian S. A. 4'-Hydroxystyryldiazines: Synthesis and Fluorescence Properties. 1995. **51**: 1585–1598.
doi: 10.1016/0040-4020(94)01050-A
7. Perkampus H.-H., Bluhm T. Zurphotochemie der styryldiazine: Darstellung der Edukte und Produkte. *Tetrahedron*. 1972. **28**: 2099–2110.
doi: 10.1016/0040-4020(72)88017-7
8. Hurst D. T., Beautont C., Jones D.T.E., Kingsley D.A., Partridge J.D., Rutherford T. The Chemistry of Pyrimidinethiols. II. The Preparation and Reactions of Some 2-Arenecarbonylmethylthiopyrimidines. *J. Aust. J. Chem.* 1988. **41**: 1209–1219.
doi: 10.1071/CH9881209
9. Stepanov D.E., Grishuk L.V., Ivanov R.Yu., Yavolovskii A.A., Kamalov G.L. A simple approach to the synthesis of 2-(2-amino-4-arilthiazol-5-yl)pyrimidines. *Rus. J. Gen. Chem.* 2013. **N3** (83): 526–529.
doi: 10.1134/S1070363213030195

Стаття надійшла 15.01.2025.

UDC 546.26-162: 541.13:549.21 doi: 10.33609/2708-129X.91.3.2025.34-48

ENANTIOMER PURIFICATION THROUGH ACHIRAL CHROMATOGRAPHY: INTEGRATING SIMULATED MOVING BED AND SELF-DISPROPORTIONATION OF ENANTIOMERS.

Alicja Wzorek,[1] Karel D. Klika,[2] Jianlin Han,[3] Alexander E. Sorochinsky,[4] Taizo Ono,[5] Vadim A. Soloshonok [*6,7]

[1] *Institute of Chemistry, Jan Kochanowski University in Kielce, Uniwersytecka 7, 25–406 Kielce, Poland;*
[2] *Research and Development Center, Archer Daniels Midland, 1001 N Brush College Rd., Decatur, IL 62521, USA;*
[3]*Jiangsu Co-Innovation Center of Efficient Processing and Utilization of Forest Resources, College of Chemical Engineering, Nanjing Forestry University, Nanjing 210037, China;*
[4] *V.P. Kukhar Institute of Bioorganic Chemistry and Petrochemistry, The National Academy of Sciences of Ukraine, Kyiv 02094, Ukraine;*
[5] *National Institute of Advanced Industrial Science and Technology (AIST), 2266–98, Anagahora, Shimoshidami, Moriyama-ku, Nagoya, 463–8560, Japan;*
[6] *Department of Organic Chemistry I, Faculty of Chemistry, University of the Basque Country UPV/EHU, Paseo Manuel Lardizábal 3, 20018 San Sebastián, Spain;*
[7] *IKERBASQUE, Basque Foundation for Science, María Díaz de Haro 3, Plaza Bizkaia, 48013 Bilbao, Spain*
**email: vadimsoloshonok@gmail.com*

Enantiomer purification is a critical process in the pharmaceutical, agrochemical, and food industries, where chiral compounds often exhibit distinct biological activities. Traditional chiral chromatography is effective but costly due to the use of expensive chiral stationary phases. This review article highlights a recent breakthrough in enantiomer purification under entirely achiral conditions. Specifically, it focuses on the convergence of achiral simulated moving bed chromatography and the phenomenon of self-disproportionation of enantiomers (SDE). Experimental validation using scalemic methyl p-tolyl sulfoxide as a model compound enabled the isolation of the excess enantiomer with high purity (~99% ee) and a respectable yield (~50%). This innovative process features exceptional productivity (up to 99 grams per liter of column volume per day), reproducibility, and reliability. This breakthrough presents the first practical example of enantiomer purification based on SDE, offering a scalable and economically viable alternative to conventional chiral separations. Given that SDE is an inherent property of all chiral compounds, this innovative approach is anticipated to become the method of choice for practical enantiomer purification in both research and industrial production.

Key words: Chirality, Enantiomers, Purification, Self-Disproportionation of Enantiomers (SDE), Achiral Chromatography, Simulated Moving Bed Chromatography.

INTRODUCTION. Chiral compounds play a crucial role in the pharmaceutical, agrochemical, and food industries [1–6]. Incorporating elements of chirality, particularly a stereogenic carbon, in compounds under development enhances the success rate of these molecules as they progress from the discovery phase to approval [7]. Approximately 70% of approved drugs on the pharmaceutical market contain at least one element of chirality [8]. Following the Thalidomide tragedy [9–11], the FDA mandates a separate full biological study for each enantiomer of submitted chiral compounds. Asymmetric synthesis, whether stoichiometric, catalytic, or enzymatic, very rarely affords chiral compounds with the level of enantiomeric purity required for the FDA-mandated biological study [12]. Incredibly, the final enantiomer purification stage can be the most laborious and costly phase of the entire chemical procedure [13, 14]. Therefore, the ability to isolate pure enantiomers becomes an absolutely essential part of successful drug development, ensuring reasonable time and cost structures.

Traditional enantiomer separation techniques, such as chiral chromatography (CCh) and diastereoisomeric crystallization, grapple with challenges like high costs and the unpredictably complex selection of resolving agents and conditions [15–18]. However, a recent study led by Professor Dorota Antos [19] has achieved a significant breakthrough by merging two previously orthogonal innovations in the fields of chirality and chromatographic separations.

The first innovation is the self-disproportionation of enantiomers (SDE) [20, 21], which allows for the separation of excess enantiomers from the racemic portion under completely achiral conditions. The second is simulated moving bed (SMB) chromatography, currently the most efficient solution for continuous chromatographic separation [2, 23].

This newly reported approach – achiral SMB (ACh-SMB) – undoubtedly deserves special attention and widespread dissemination among practitioners in the areas of chirality, chromatography, asymmetric synthesis, and drug development in academic and industrial research institutions. Given the high methodological and practical potential of these results, this brief Perspective aims to highlight the reported methodological and technological advances, situating them within the greater concept of the SDE phenomenon. These recent developments bode well for the future general applications of ACh-SMB-SDE as an approach of choice in enantiomer purifications.

Self-disproportionation of enantiomers (SDE). As illustrated in Fig. 1, a scalemic mixture of 6 red and 3 blue enantiomers can adopt five general configurations based on intermolecular interactions. In configuration **A**, where such interactions are absent or very weak, all nine molecules in an achiral environment will behave congruently, requiring a chiral selector to distinguish between red and blue enantiomers. However, when intermolecular interactions occur, describing a scalemic compound merely as a mixture of enantiomers becomes conceptually incorrect and methodologically misleading. Thus, if there is a preference for heterochiral interactions, the sample should be described as a collection of dimers (**B**) or oligomers (**E**) along with the corresponding monomers. Conversely, if homochiral intermolecular interactions dominate, the molecular configurations will include dimers versus monomers (**C**) and a mixture of oligomers (**D**)

with molecular weight distributions reflecting the ratio of the original enantiomers. These four molecular configurations, driven by intermolecular interactions, are essentially mixtures of compounds with different molecular weights and distinct physicochemical properties, resulting in their separation in a completely achiral environment. This spontaneous separation of scalemic samples into fractions with proportions of enantiomers different from the original mixture is termed Self-Disproportionation of Enantiomers (SDE) [24–26].

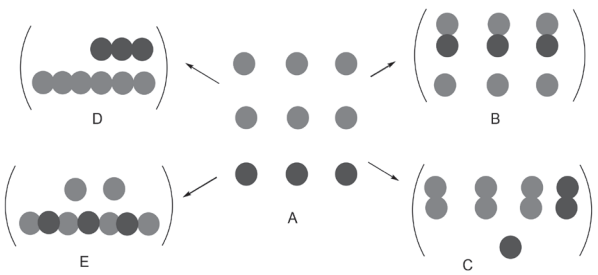

Fig. 1. Scalemic mixture of 33.33% ee and four general configurations: absence of any intermolecular interactions (A); intermolecular interactions leading to the formation of heterochiral dimers (B), homochiral dimers (C), homochiral oligomers (D), and heterochiral oligomers (E).

Since intermolecular interactions are an inherent property of all chemical compounds, one can deduce that SDE is similarly an inherent property of all chiral compounds. Systematic research into SDE began only about 20 years ago, generating a wealth of SDE data for compounds of various chemical structures and all common types of chirality, including helical [27], axial [28–34] chirality, central chirality on carbon [35–37], sulfur [38–41], as well as compounds possessing multiple stereogenic centers and C_2 symmetry [42]. A similar wide generality is also reported for areas of SDE manifestation, particularly in crystallization [43, 44], sublimation [45–48], distillation [49–51], density gradient ultracentrifugation [52] or suspension precipitation [53], and chromatography – including simple gravity-driven columns [54–56], flash chromatography [38], MPLC [57–59], HPLC [28], size-exclusion [51], and even gas chromatography [60].

Among the wider implications of the ubiquitous nature of SDE is the problem of accurately reporting the enantiomeric purity of chiral compounds isolated from natural sources or prepared in the laboratory [61–63]. SDE is highly relevant to the field of chirality and asymmetric synthesis. Understanding SDE is crucial for accurately reporting the stereochemical outcomes of enantioselective reactions. SDE presents both a challenge and an opportunity in chemistry, requiring careful consideration and control to avoid errors in experimental results and interpretation [64–66].

A particularly exciting implication of SDE is related to the origin of prebiotic homochirality. Among various theories proposed, SDE is the only experimentally proven mechanism for the formation and maintenance of enantiomerically pure or highly enriched samples [67–69].

SDE and enantiomer purifications. In essence, the SDE phenomenon is the spontaneous separation of the excess enantiomer from the racemic portion. Therefore, enantiomer purification is an innate property and the way of SDE manifestation. Thus, the primary question is how to amplify this spontaneous, innate enantiomer purification to a practical application level. Research conducted on numerous chiral compounds has identified certain structural classes and functional groups, known as SE-phoric groups [21, 70], that allow for high magnitudes of SDE, reaching prac-

tical levels. As SDE can be used as a method to obtain enantiopure samples from scalemic mixtures, it can lead to the development of unconventional and superior methods for enantiopurification. Particularly exciting results were reported for the SDE-driven enantiomer purification via sublimation [71–75] and achiral column chromatography. Figure 2 and Table 1 present several examples of various types of chiral organic compounds.

Table 1. Examples of SDE-driven enantiomer purifications via achiral chromatography.

Entry	**Cmpd.**	**Starting ee [%]**	**Type of chromatography**	**Eluent**	**First fraction [%]**	**Last fraction [%]**	**Δee**	**Yields [%]**
1	**1**	75.0 (*S*)	flash	*c*-Hex–benzene–di-*tert*-butyl ether (1:1:0.1)	28.0	>99	63.3	44.0
2	**2**	78.9 (*S*)	gravity	*c*-Hex/MTBE (1:2)	>99	56.6	43.3	24.0
3	**2**	71.0 (*S*)	MPLC	*n*-Hex–EtOAc (1:1)	>99	28	71	66.0
4	**3**	64.9 (*R*)	gravity	*c*-hex/MTBE (1:2)	>99	33.2	66.7	21.7
5	**4**	72.6 (*S*)	gravity	*c*-hex/MTBE (1:2)	80.3	79.9	12.6	–
6	**4**	69.0 (*S*)	MPLC	*n*-Hex–EtOAc (2:1)	>99	52.0	47	40.0
7	**5**	64.2 (*P*)	gravity	CH_2CL_2	>99	44.6	55.3	0.7
8	**5**	65.8 (*P*)	MPLC	*n*-Hex–EtOAc	>99	35.4	63.6	53.6
9	**6**	34.6 (*R*)	gravity	*n*-Hex–EtOAc (5:1)	8.1	>99	91.8	4.3
10	**7**	34.6 (*R*)	gravity	*c*-Hex/EtOAc (1:5)	>99	13.0	86	0.5
11	**8**	81.4 (S)	flash	*n*-Hex–EtOAc	93.5	62.3	31.2	–
12	**9**	72.4 (*S*)	gravity	*n*-Hex–EtOAc (1:13)	97.0	47.4	49.6	–
13	**10**	82 (*M*)	gravity	*n*-Hex–EtOAc (3:1)	69	89	20	–

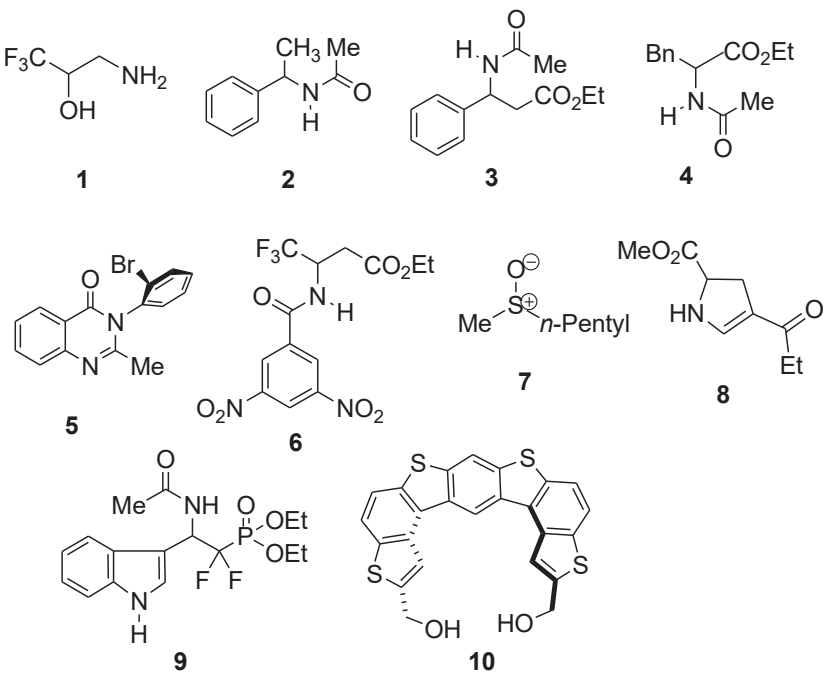

Fig. 2. Examples of compounds exhibiting a high magnitude of self-disproportionation of enantiomers (SDE) under achiral chromatography conditions.

Examples **1**–**10** (Fig.1) were selected to showcase the structural variety of chiral compounds demonstrating significant SDE magnitudes, leading to laboratory-scale enantiomer purifications. These examples include unprotected amino alcohol **1** [76], amide-protected amine **2** [55, 77, 78], α-amino acid **4** [79], β-amino acids **3** [54, 57, 80] and **6** [37], phosphorus analog of β-amino acid **9** [81], unprotected α-amino ester **8** [82], sulfoxide **7** [39], compound with axial chirality **5** [83], and helicine **10** [27].

For each compound (**1**–**10**), Table 1 provides data on initial enantiomeric purity, type of achiral chromatography, eluent, enantiomeric excess in the first and last fractions, the difference in enantiomeric excess (Δee), and the yields of isolated enantiomerically pure compounds. These data overwhelmingly highlight the prowess of SDE via achiral chromatography as a general approach for the enantiopurification of scalemic organic compounds. However, practical application has been severely hindered by difficulties in scaling up from gram to a practically useful level of 100 g or more. This is why the breakthrough reported by Dorota Antos' group [19] represents a critically needed advancement in this field.

Simulated moving bed chromatography. Simulated Moving Bed (SMB) chromatography is an advanced technique used to separate and purify different components from a mixture [84-87]. Unlike traditional batch chromatography, which processes samples in fixed amounts, SMB operates continuously, making it more efficient and cost-effective for large-scale separations. SMB chromatography consists of several interconnected columns filled with a sta-

tionary phase that interacts uniquely with each component of the mixture. A liquid containing the mixture flows through the system, and the continuous alternation of input and output positions facilitates the separation process, replicating the effect of a moving solid phase. The number of columns typically used can vary depending on the specific application and scale of the process. Generally, 8, 12, or 16 columns are commonly employed. Simplified version of the SMB system is illustrated in Fig. 2.

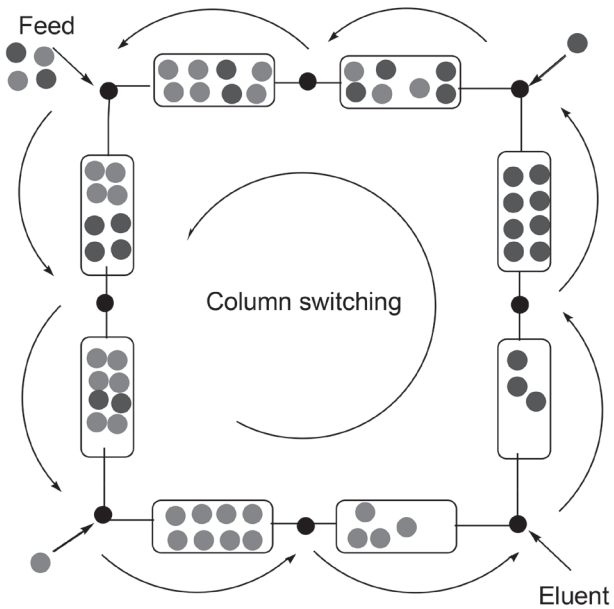

Fig. 2. Schematic of SMB units separating a binary mixture.

SMB consists of several connected columns filled with a stationary material that interacts differently with each component of the mixture. A liquid carrying the mixture flows through the system, and due to the constant switching of input and output positions, the separation process mimics the effect of a moving solid phase [88–90].

SMB is widely used in industries like pharmaceuticals, food processing, and petrochemicals [91-95]. It offers several benefits such as higher efficiency, better purity, and cost-effectiveness. SMB is widely used in pharmaceutical industry for large-scale isolation/purification of drug components, especially enantiomers in chiral drugs. In food industry for refining sugars, amino acids, and other food additives. More generally, in chemical industry for separation of petrochemical products and bio-based chemicals. Overall, while SMB chromatography may seem complex, it is essentially a smart way of continuously filtering out desired compounds from mixtures. By improving efficiency and reducing waste, it plays a crucial role in modern industry and scientific research.

Case of methyl p-tolyl sulfoxide. The study under discussion [19] focused on developing an SDE-driven Achiral Simulated Moving Bed (SDE-ACh-SMB) process for the separation of enantiomers of (*S*)-MTSO (Scheme 1).

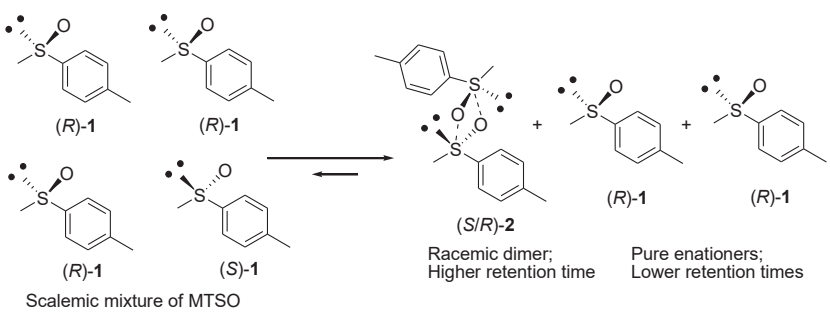

Scheme 1. SDE-driven enantiopurification of scalemic S-MTSO.

Due to identical Henry constants for enantiomers in an achiral environment, conventional design methods like triangle theory were inapplicable [96–98]. Instead, the approach involved three steps, including batch-column separation for model calibration, model-aided selection of operational variables, and experimental adjustment.

Elution experiments helped determine key parameters such as total column porosity (εt), apparent dispersion coefficient (Da), and isotherm coefficients (qm, KI, KII). The porosity (εt) averaged 0.70 with minimal deviations between columns. The number of theoretical plates (N ≈ 1000) was used to calculate Da, and the isotherm coefficients were estimated using peak fitting techniques. These parameters ensured accurate predictions of migration velocities for the enantiomers' fronts during the separation process.

Initial experiments in batch columns demonstrated the SDE phenomenon, allowing the formation of homochiral and heterochiral associates with different retention properties.

Optimal conditions for batchwise achiral separation were determined, providing a baseline for further SMB experiments.

A series of SMB runs were conducted with varying zone flowrates, switching times, and feed conditions. The initial scouting run failed due to incorrect predictions of enantiomer migration velocities.

Subsequent runs adjusted flowrates and switching times, achieving high-purity separation of S-MTSO enantiomer with improved productivity and yield. Specifically, run 3 reached approximately 100% purity with a productivity of 28 grams of (*S*)-MTSO per liter of column volume per day.

Variations in feed concentration and enantiomeric excess were investigated. Higher ee improved product purity and productivity by enhancing the migration velocity difference between enantiomers. Increased feed concentration intensified the SDE effect, beneficial for separation performance, but also made maintaining product purity more challenging due to the sharper concentration fronts of enantiomers.

The dynamic model was verified against experimental data, confirming its accuracy and reliability in predicting SMB separation performance. The model parameters were adjusted based on experimental results to ensure precise predictions.

The ACh-SMB system used for the enantiopurification was equipped with four Smartline Pumps (model 100 V.5010), a pair of UV detectors (K-2501), an SMB-Control unit, and a multifunctional valve (CSEP C9 Series Simulated Moving Bed and Chromatography Systems V0499, 12/2000). All components were sourced from Knauer.

In showcase experiments the enantiomeric excess (ee) of the enantioenriched MTSO stream was maintained at 50%. The yield of the target enantiomer (S-MTSO) was approximately 26%. The productivity was 28 grams of S-MTSO per liter of total column volume per day. These experiments clearly highlighted the key benefits and effectiveness of the method, providing clear and compelling evidence of its capabilities. The reproducibility of the ACh-SMB process was confirmed through repeated runs, yielding consistent performance indicators.

The developed ACh-SMB process offers a cost-effective alternative for separating non-racemic mixtures with high ee, common in asymmetric synthesis. This method can reduce reliance on expensive chiral chromatography. For mixtures with low ee, a tandem configuration with chiral chromatography can improve

process economy by recycling the waste fraction.

CONCLUSIONS. A novel SDE-ACh-SMB process was developed and verified for the continuous separation of enantiomers from nonracemic mixtures [19]. The process is feasible, reproducible, and predictable, demonstrating high potential for industrial applications. Optimal conditions achieved product purity of 96–100% and productivity up to 99 grams per liter of column volume per day. The only drawback of this method is the remaining racemic compound, which must be discarded or resolved using an external chiral selector. In this regard, one can envision an advanced methodology presented in Fig. 3. The process starts with a racemic compound. Using low-cost chiral chromatography, the racemate is transformed into two fractions of scalemic compounds, enantiomerically enriched in (R)- and (S)-enantiomers, respectively. Next, the SDE-SMB approach is used to separate the target enantiomers, and the remaining portion is fed back to the racemate injector port. Properly designed and working continuously, such a process will revolutionize the separation of enantiomers.

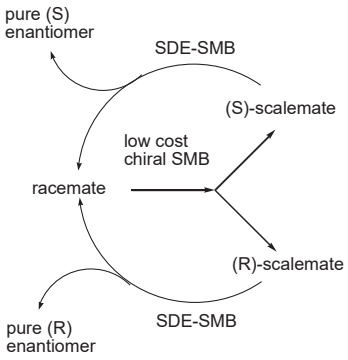

Fig. 3. Proposed advanced process for resolution of racemates using low-cost chiral chromatography and the SDE-SMBCh.

Since SDE is an inherent property of all chiral compounds, the SDE-ACh-SMB process is expected to have the broadest possible applicability in the field of enantiomer purifications.

ОЧИЩЕННЯ ЕНАНТІОМЕРІВ ЗА ДОПОМОГОЮ АХІРАЛЬНОЇ ХРОМАТОГРАФІЇ: ІНТЕГРАЦІЯ СИМУЛЬОВАНОГО РУХОМОГО ШАРУ ТА САМОДИСПРОПОРЦІОНУВАННЯ ЕНАНТІОМЕРІВ

Аліція Взорек,[1] Карел Д. Кліка,[2] Джіанлін Хань,[3] Олександр Е. Сорочинський,[4] Тайзо Оно,[5] Вадим А. Солошонок[6,7]*

[1] Інститут хімії, Університет Яна Кохановського в Кельцях, вул. Університетська 7, 25–406 Кельце, Польща;

[2] Центр досліджень і розроблень, Archer Daniels Midland, 1001 N Brush College Rd., Декейтер, Іллінойс 62521, США;

[3] Цзянсу Співдружній центр ефективного оброблення і використання лісових ресурсів, Коледж хімічного машинобудування, Нанкінський лісовий університет, Нанкін 210037, Китай;

[4] Інститут біоорганічної хімії та нафтохімії ім. В. П. Кухаря, Національна академія наук України, вул. Академіка Кухаря, 1, Київ 02094, Україна;

[5] Національний інститут передових промислових наук і технологій (AIST), 2266–98, Анагагора, Шимошидамі, Моріяма-ку, Нагоя, 463–8560, Японія;

[6] Кафедра органічної хімії I, Факультет хімії, Університет Країни Басків UPV/EHU, Пасаео Мануель Лардісабаль 3, 20018 Сан Себастьян, Іспанія;

[7] IKERBASQUE, Баскський фонд науки, вул. Марія Діас де Харо 3, площа Бізкая, 48013 Більбао, Іспанія

Очищення енантіомерів є важливим процесом у фармацевтичній, агрохімічній та харчовій промисловості, де хіральні сполуки часто виявляють різну біологічну активність. Традиційна хіральна хроматографія є ефективною, але дорогою через використання дорогих хіральних стаціонарних фаз. Ця оглядова стаття висвітлює останній прорив у очищенні енантіомерів в умовах повністю ахіральних умов. Зокрема, акцент зроблено на поєднанні ахіральної симульованої рухомої шарової хроматографії та феномена самодиспропорціонування енантіомерів (SDE). Експериментальна перевірка з використанням скалемічного метил-р-толуїлсульфоксиду як модельної сполуки дозволила ізолювати надлишковий енантіомер із високою чистотою (~99% ее) та поважним виходом (~50%). Цей інноваційний процес характеризується винятковою продуктивністю (до 99 грамів на літр об'єму колони на день), відтворюваністю та надійністю. Цей прорив являє собою перший практичний приклад очищення енантіомерів на основі SDE, пропонуючи масштабовану та економічно доцільну альтернативу традиційним хіральним розділенням. Враховуючи, що SDE є властивістю всіх хіральних сполук, цей інноваційний підхід очікувано має стати пріоритетним методом для практичного очищення енантіомерів як у дослідженнях, так і в промисловому виробництві.

Ключові слова: хіральність, енантіомери, очищення, самодиспропорціонування енантіомерів (SDE), ахіральна хроматографія, симульована рухома шарова хроматографія.

REFERENCES

[1] Hutt A. J., Tan S. C. Drug Chirality and its Clinical Significance. *Drugs*. 1996. **52** (Suppl 5): 1–12. doi.org/10.2165/00003495-199600525-00003.

[2] Lin G. Q., You Q. D., Cheng J. F. *Chiral drugs*. In *Chemistry and Biological Action*. Wiley. 2011. doi:10.1002/9781118075647.

[3] Brooks W. H., Guida W. C., Daniel K. G. The significance of chirality in drug design and development. *Curr. Top. Med. Chem*. 2011. **11**(7): 760–770. doi: 10.2174/156802611795165098.

[4] Ceramella J., Iacopetta D., Franchini A. *et al*. A look at the importance of chirality in drug activity: Some significative examples. *Appl. Sci*. 2022. **12**(21): 10909. doi.org/10.3390/app122110909.

[5] Crossley R. J. *Chirality and biological activity of drugs*. CRC Press. 1995.

[6] Jianlin Han, Alicja Wzorek, Gagan Dhawan, Wei Zhang, Alexander E. Sorochinsky, Daniel Baecker, Taizo Ono, Karel D. Klika Vadim A. Soloshonok. Chiral fluorine-containing pharmaceuticals. *Ukr. Chim. J*. 2024. 91(2): 55–90.

[7] Lovering F., Bikker J., Humblet C. Escape from Flatland: Increasing Saturation as an Approach to Improving Clinical Success. *J. Med. Chem*. 2009. **52**(21): 6752–6756. doi.org/10.1021/jm901241e.

[8] Calcaterra A., D'Acquarica I. The market of chiral drugs: Chiral switches versus de novo enantiomerically pure compounds. *J. Pharmaceut. Biomed. Anal*. 2018. **147**: 323–340. doi.org/10.1016/j.jpba.2017.07.008.

[9] Kim J.H, Scialli A.R. Thalidomide: the tragedy of birth defects and the effective treatment of disease. *Toxicological sciences*. 2011. **122**(1): 1–6. https://doi.org/10.1093/toxsci/kfr088.

[10] Annas G.J., Elias S. Thalidomide and the Titanic: reconstructing the technology tragedies of the twentieth century. *American journal of public health*. 1999. **89**(1): 98–101. https://doi.org/10.2105/AJPH.89.1.98.

[11] Yamada T., Okada T., Sakaguchi K. *et al*. Efficient asymmetric synthesis of novel 4-substituted and configurationally stable analogues of thalidomide. *Org. Lett*. 2006. **8**(24): 5625–5628.
doi: 10.1021/ol0623668.
[12] De Camp W.H. Chiral drugs: the FDA perspective on manufacturing and control. *Journal of pharmaceutical and biomedical analysis*. 1993. **11**(11–12): 1167–1172.
https://doi.org/10.1016/0731-7085(93)80100-F.
[13] Rekoske J.E. Chiral separations. American Institute of Chemical Engineers. *AIChE Journal*. 2001. **47**(1): 2. 7327e0c2d7bbd609c9557102213c3c60.
[14] Sui J., Wang N., Wang J. *et al*. Strategies for chiral separation: from racemate to enantiomer. *Chemical Science*. 2023. **14**(43): 11955–2003. DOI: 10.1039/D3SC01630G.
[15] Wu D., Pan F., Tan W. *et al*. Recent progress of enantioseparation under scale production (2014–2019). *Journal of separation science*. 2020. **43**(1): 337–347.
https://doi.org/10.1002/jssc.201900682.
[16] Leek H., Thunberg L., Jonson A.C. *et al*. Strategy for large-scale isolation of enantiomers in drug discovery. *Drug Discovery Today*. 2017. **22**(1): 133–139.
https://doi.org/10.1016/j.drudis.2016.09.018.
[17] Francotte E.R. Enantioselective chromatography as a powerful alternative for the preparation of drug enantiomers. *Journal of Chromatography A*. 2001. **906**(1–2): 379–397.
https://doi.org/10.1016/S0021-9673(00)00951-1.
[18] Lorenz H., Seidel-Morgenstern A. Processes to separate enantiomers. *Angewandte Chemie International Edition*. 2014. **53**(5): 1218–1250.
https://doi.org/10.1002/anie.201302823.
[19] Marek W.K., Lee J.W., Seidel-Morgenstern A., Antos D. Separation of nonracemic mixtures of enantiomers by achiral simulated moving bed chromatography. *Separation and Purification Technology*. 2025. **361**: 131497.
doi.org/10.1016/j.seppur.2025.131497.
[20] Han J., Kitagawa O., Wzorek, A. *et al*. The self-disproportionation of enantiomers (SDE): a menace or an opportunity? *Chem. Sci*. 2018. **9**: 1718–1739,
DOI: 10.1039/C7SC05138G.
[21] Soloshonok V. A., Klika K. D. Terminology Related to the Phenomenon 'Self-Disproportionation of Enantiomers' (SDE), *Helv. Chem Acta*, 2014. **97**: 1583–1589.
DOI: 10.1002/hlca.201400122.
[22] Juza M., Mazzotti M., Morbidelli M. Simulated moving-bed chromatography and its application to chirotechnology. *Trends in biotechnology*. 2000. **18**(3): 108–18.
DOI: 10.1016/S0167-7799(99)01419-5.
[23] Seidel-Morgenstern A., Kessler L.C., Kaspereit M. New developments in simulated moving bed chromatography. Chemical Engineering & Technology: Industrial Chemistry-Plant Equipment-Process *Engineering-Biotechnology*. 2008. **31**(6): 826–37.
https://doi.org/10.1002/ceat.200800081.
[24] Soloshonok V.A. Remarkable amplification of the self-disproportionation of enantiomers on achiral-phase chromatography columns. *Angewandte Chemie International Edition*. 2006. **45**(5): 766–769.
doi.org/10.1002/anie.200503373.
[25] Soloshonok V.A., Berbasov D.O. Self-disproportionation of enantiomers on achiral phase chromatography. One more example of fluorine's magic powers. *Chim. Oggi Chem. Today*. 2006. **24**: 44–47.
[26] Soloshonok V.A., Roussel C., Kitagawa O., Sorochinsky A.E. Self-Disproportionation of Enantiomers via Achiral Chromatography: a Warning and Extra Dimension in Optical Purifications, *Chem. Soc. Rev*. 2012. **41**: 4180–4188.
DOI:10.1039/C2CS35006H.
[27] Tanaka K., Osuga H., Suzuki H. *et al. J. Chem. Soc., Perkin Trans. 1*. 1998. 935–940.
DOI: 10.1039/A707196E.
[28] Matusch R., Coors C. Chromatographic separation of the excess enantiomer under achiral

conditions. *Angewandte Chemie International Edition in English*. 1989. **28**(5): 626–627. doi.org/10.1002/anie.198906261.

[29] Nicoud R.M., Jaubert J.N., Rupprecht I., Kinkel J. Enantiomeric enrichment of non-racemic mixtures of binaphthol with non-chiral packings. *Chirality*. 1996. **8**(3): 234–243. doi.org/10.1002/(SICI)1520-636X(1996)8:3<234::AID-CHIR2>3.0.CO;2-H.

[30] Baciocchi R., Zenoni G., Mazzotti M., Morbidelli M. Separation of binaphthol enantiomers through achiral chromatography. *Journal of Chromatography A*. 2002. **944**(1–2): 225–240. doi.org/10.1016/S0021-9673(01)01366-8.

[31] Baciocchi R., Mazzotti M., Morbidelli M. General model for the achiral chromatography of enantiomers forming dimers: application to binaphthol. *Journal of Chromatography A*. 2004. **1024**(1–2): 15–20. doi.org/10.1016/j.chroma.2003.10.071.

[32] Nakajima M., Kanayama K., Miyoshi I., Hashimoto S.I. Catalytic asymmetric synthesis of binaphthol derivatives by aerobic oxidative coupling of 3-hydroxy-2-naphthoates with chiral diamine-copper complex. *Tetrahedron letters*. 1995. **36**(52): 9519–9520. doi.org/10.1016/0040-4039(95)02063-2.

[33] Nakajima M., Miyoshi I., Kanayama K. *et al.* Enantioselective Synthesis of Binaphthol Derivatives by Oxidative Coupling of Naphthol Derivatives Catalyzed by Chiral Diamine-Copper Complexes. *J. Org. Chem*. 1999. **64**(7): 2264–71. doi.org/10.1021/jo981808t.

[34] Takahashi M., Tanabe H., Nakamura T. *et al.* Atropisomeric lactam chemistry: catalytic enantioselective synthesis, application to asymmetric enolate chemistry and synthesis of key intermediates for NET inhibitors. *Tetrahedron*. 2010. **66**(1): 288–96. doi.org/10.1016/j.tet.2009.10.095.

[35] Cundy K.C., Crooks P.A. Unexpected phenomenon in the high-performance liquid chromatographic analysis of racemic 14C-labelled nicotine: Separation of enantiomers in a totally achiral system. *Journal of Chromatography A*. 1983. **281**: 17–33. https://doi.org/10.1016/S0021-9673(01)87863-8.

[36] Charles R., Gil-Av E. Self-amplification of optical activity by chromatography on an achiral adsorbent. *Journal of Chromatography A*. 1984. **298**: 516–20. doi.org/10.1016/S0021-9673(01)92750-5.

[37] Soloshonok V.A., Berbasov D.O. Self-disproportionation of enantiomers of (R)-ethyl 3-(3, 5-dinitrobenzamido)-4, 4, 4-trifluorobutanoate on achiral silica gel stationary phase. *J. Fluor. Chem*. 2006. **127**(4–5): 597–603. doi.org/10.1016/j.jfluchem.2005.11.004.

[38] Diter P., Taudien S., Samuel O., Kagan H.B. Enantiomeric enrichment of sulfoxides by preparative flash chromatography on an achiral phase. *J. Org. Chem*. 1994. **59**(2): 370–373. doi.org/10.1021/jo00081a015.

[39] Wzorek A., Klika K.D., Drabowicz J. *et al.* The self-disproportionation of the enantiomers (SDE) of methyl n-pentyl sulfoxide via achiral, gravity-driven column chromatography: a case study, *Org. Biomol. Chem*. 2014. **12**: 4738–4746, DOI: 10.1039/c4ob00831f.

[40] Drabowicz J., Jasiak A., Wzorek A. *et al.* Self-disproportionation of enantiomers (SDE) of chiral sulfoxides, amides and thioamides via achiral chromatography, *Arkivoc* 2017. 557–578. DOI: 10.3998/ark.5550190.0018.200.

[41] Han J., Soloshonok V.A., Klika K. D. *et al.* Chiral sulfoxides: advances in asymmetric synthesis and problems with the accurate determination of the stereochemical outcome, *Chem. Soc. Rev*. 2018. **47**: 1307–1350. DOI: 10.1039/c6cs00703a.

[42] Takahata H., Takahashi S., Kouno S.I., Momose T. Symmetry-Assisted Synthesis of C 2-Symmetric trans-α, α ʻ-Bis (hydroxymethyl) pyrrolidine and-piperidine Derivatives via Double Sharpless Asymmetric Dihydroxylation of α, ω-Terminal Dienes. *J. Org. Chem*. 1998. **63**(7): 2224–31. doi.org/10.1021/jo971995f.

[43] Secor R.M. Resolution of Optical Isomers by Crystallization Procedures. *Chem. Rev*. 1963. **63**(3): 297–309. doi.org/10.1021/cr60223a006.
[44] Fogassy E., Nógrádi M., Kozma D. *et al*. Optical resolution methods. *Org. Biomol. Chem*. 2006. **4**(16): 3011–30. doi.org/10.1039/B603058K.
[45] Soloshonok V.A., Ueki H., Yasumoto M. *et al*. Phenomenon of optical self-purification of chiral non-racemic compounds. J. Am. Chem. Soc. 2007. **129**(40): 12112–12113. doi.org/10.1021/ja065603a.
[46] Pracejus G. Optical Activation of N-Phthalyl-α-Amino Acid Derivatives by Tertiary Base Catalysis. *Lieb. Ann. Chem*. 1959. **622**(1): 10–22. doi.org/10.1002/jlac.19596220104.
[47] Kwart H., Hoster D.P. Separation of an enantiomorph and its racemate by sublimation. *J. Org. Chem*. 1967. **32**(6): 1867–70. doi.org/10.1021/jo01281a037.
[48] Garin D.L., Greco D.J., Kelley L. Enhancement of optical activity by fractional sublimation. An alternative to fractional crystallization and a warning. J. Org. Chem. 1977. **42**(7): 1249–1251. doi.org/10.1021/jo00427a033.
[49] Katagiri T., Yoda C., Furuhashi K. *et al*. Separation of an enantiomorph and its racemate by distillation: strong chiral recognizing ability of trifluorolactates. *Chem. Lett*. 1996. **25**(2): 115–116. doi.org/10.1246/cl.1996.115.
[50] Katagiri T., Takahashi S., Tsuboi A. *et al*. Discrimination of enantiomeric excess of optically active trifluorolactate by distillation: Evidence for a multi-center hydrogen bonding network in the liquid state. *J. Fluor. Chem*. 2010. **131**(4): 517–520. doi.org/10.1016/j.jfluchem.2009.12.007.
[51] Aceña J.L., Sorochinsky A.E., Katagiri T., Soloshonok V.A. Unconventional preparation of racemic crystals of isopropyl 3,3,3-trifluoro-2-hydroxypropanoate and their unusual crystallographic structure: the ultimate preference for homochiral intermolecular interactions, *Chem. Commun.*, 2013. **49**: 373–375; DOI: 10.1039/c2cc37491a.
[52] Mastai Y., Völkel A., Cölfen H. Separation of racemate from excess enantiomer of chiral nonracemic compounds via density gradient ultracentrifugation. *J. Am. Chem. Soc*. 2008. **130**(8): 2426–2427. doi.org/10.1021/ja067905i.
[53] Kozma D., Kassai C., Fogassy E. Enantiomeric enrichment by the use of density differences between racemic compounds and optically active enantiomers. *Tetrahedron Lett*. 1995. **36**(18): 3245–3246. doi.org/10.1016/0040-4039(95)00454-K
[54] Suzuki Y., Han J., Kitagawa O. *et al*. A comprehensive examination of the self-disproportionation of enantiomers (SDE) of chiral amides via achiral, laboratory-routine, gravity-driven column chromatography. *RSC Adv*. 2015. **5**(4): 2988–2993. doi: 10.1039/C4RA13928C.
[55] Wzorek A., Sato A., Drabowicz J. *et al*. Enantiomeric enrichments via the self-disproportionation of enantiomers (SDE) by achiral, gravity-driven column chromatography: a case study using N-acetyl-1-(phenyl)ethylamine for optimizing the enantiopure yield and magnitude of the SDE, *Helv. Chem Acta*, 2015. **98**: 1147–1159. DOI: 10.1002/hlca.201500041.
[56] Wzorek A., Sato A., Drabowicz J., Soloshonok V. A. Self-Disproportionation of Enantiomers via achiral gravity-driven column chromatography: a case study of N-Acyl-α-Phenylethylamines, *J. Chromatog. A*. 2016. **1467**: 270–278. DOI: 10.1016/j.chroma.2016.05.044.
[57] Nakamura T., Tateishi K., Tsukagoshi S. *et al.* Self-disproportionation of enantiomers of non-racemic chiral amine derivatives through achiral chromatography. *Tetrahedron*. 2012. **68**(21): 4013–4017. doi:10.1016/j.tet.2012.03.054.
[58] Tateishi K., Tsukagoshi S., Nakamura T. *et al.*

Chiral initiator-induces self-disproportionation of enantiomers via achiral chromatography: application to enantiomer separation of racemate, *Tetrahedron Lett*. 2013. **54**: 5220–5223.
DOI: 10.1016/j.tetlet.2013.07.061.

[59] Goto M., Tateishi K., Ebine K. *et al*. Chiral additive induced self-disproportionation of enantiomers under MPLC conditions: Preparation of enantiomerically pure samples of 1-(aryl)ethylamines from racemates, *Tetrahedron: Asymmetry*, 2016. 27: 317–321.
DOI: 10.1016/j.tetasy.2016.03.004.

[60] Wzorek A., Soloshonok V.A., Klika K.D. The Self-Disproportionation of Enantiomers (SDE) of α-Pinene via Evaporation off Silica Gel and Foam Fractionation – Validation of the Plausibility of SDE via Gas Chromatography (GC) for α-Pinene, *Separations* 2023. **10**: 382.
doi.org/10.3390/ separations10070382.

[61] Han J., Wzorek A., Soloshonok V.A., Klika K.D. The self-disproportionation of enantiomers (SDE): the effect of scaling down, potential problems versus prospective applications, possible new occurrences, and unrealized opportunities? *Electrophoresis*, 2019. **40**: 1869–1880.
DOI: 10.1002/elps.201800414.

[62] Kwiatkowska M., Wzorek A., Kolbus A. *et al*. Flurbiprofen: A Study of the Behavior of the Scalemate by Chromatography, Sublimation, and NMR, *Symmetry* 2021. 13: 543.
doi.org/ 10.3390/sym13040543.

[63] Soloshonok V.A., Wzorek A., Klika K.D. A question of policy: should tests for the self-disproportionation of enantiomers (SDE) be mandatory for reports involving scalemates? *Tetrahedron: Asymmetry*. 2017. **28**(10): 1430–1434.
doi: 10.1016/j.tetasy.2017.08.020.

[64] Han J., Dembinski R., Soloshonok V. A., Klika K. D. A call for a change in policy regarding the necessity for SDE tests to validate the veracity of the outcome of enantioselective syntheses, the inherent chiral state of natural products, and other cases involving enantioenriched samples. *Molecules*. 2021. **26**(13): 3994.
doi.org/10.3390/molecules26133994.

[65] Han J., Wzorek A., Klika K. D., Soloshonok V. A. Recommended tests for the self-disproportionation of enantiomers (SDE) to ensure accurate reporting of the stereochemical outcome of enantioselective reactions. *Molecules*. 2021. **26**(9): 2757.
doi.org/10.3390/molecules26092757

[66] Han J., Wzorek A., Kwiatkowska M. *et al*. The self-disproportionation of enantiomers (SDE) of amino acids and their derivatives, *Amino Acids*, 2019. **51**: 865–889.
DOI: 10.1007/s00726-019-02729-y.

[67] Yun Y., Gellman A.J. Adsorption-induced autoamplification of enantiomeric excess on an achiral surface. *Nature Chem*. 2015. **7**(6): 520–5.
doi.org/10.1038/nchem.2250.

[68] Soai K., Kawasaki T., Matsumoto A. Role of asymmetric autocatalysis in the elucidation of origins of homochirality of organic compounds. *Symmetry*. 2019. **11**(5): 694.
doi.org/10.3390/sym11050694.

[69] Cintas P., Viedma C. On the physical basis of asymmetry and homochirality. *Chirality*. 2012. **24**(11): 894–908.
doi.org/10.1002/chir.22028.

[70] Sorochinsky A.E., Aceña J.L. Soloshonok V.A. Self-Disproportionation of Enantiomers of Chiral, Non-Racemic Fluoroorganic Compounds: Role of Fluorine as Enabling Element, *Synthesis* 2013. **45**: 141–152.
DOI: 10.1055/s-0032-1316812.

[71] Yasumoto M., Ueki H., Soloshonok V.A. Self-Disproportionation of Enantiomers of Trifluoro Lactic Acid Amides via Sublimation, *J. Fluor. Chem*. 2010. **131**: 266–269.
doi.org/10.1016/j.jfluchem.2009.10.002.

[72] Yasumoto M., Ueki H., Ono T. *et al*. Self-Disproportionation of Enantiomers via Sublimation: Isopropyl 3,3,3-(Trifluoro)-Lactate, *J. Fluor. Chem*. 2010. 131: 535–539.
doi.org/10.1016/j.jfluchem.2009.11.026.

[73] Yasumoto M., Ueki H., Soloshonok V.A. Self-disproportionation of enantiomers of α-trifluoromethyl lactic acid amides via sublimation. Journal of Fluorine Chemistry. 2010. **131**(4): 540–544. doi.org/10.1016/j.jfluchem.2009.11.010.

[74] Ueki H., Yasumoto M., Soloshonok V.A. Rational application of self-disproportionation of enantiomers via sublimation—a novel methodological dimension for enantiomeric purifications. *Tetrahedron: Asymmetry*. 2010. **21**(11–12): 1396–1400. doi.org/10.1016/j.tetasy.2010.04.040.

[75] Han J., Nelson D.J., Sorochinsky A.E., Soloshonok V.A. Self-Disproportionation of Enantiomers via Sublimation; New and Truly Green Dimension in Optical Purification, Curr. Org. Synthesis 2011. **8**: 310–317. doi.org/10.2174/157017911794697303.

[76] Sorochinsky A.E., Katagiri T., Ono T. *et al*. Optical purifications via Self-Disproportionation of Enantiomers by achiral chromatography; Case study of a series of α-CF3-containing secondary alcohols, *Chirality* 2013. **25**: 365–368. DOI: 10.1002/chir.22180.

[77] Wzorek A., Sato A., Drabowicz J., Soloshonok V.A. Self-disproportionation of enantiomers (SDE) of chiral non-racemic amides via achiral chromatography, *Israel J. Chem*. 2016. **56**: 977–989. DOI: 10.1002/ijch.201600077.

[78] Wzorek A., Kamizela A., Sato A., Soloshonok, V.A. Self-Disproportionation of Enantiomers (SDE) via achiral gravity-driven column chromatography of N-fluoroacyl-1-phenylethylamines, *J. Fluor. Chem*. 2017. **196**: 37–43. DOI: 10.1016/j.jfluchem.2016.07.016.

[79] Hosaka T., Imai T., Wzorek A. *et al*. The self-disproportionation of enantiomers (SDE) of α-amino acid derivatives; facets of steric and electronic properties, *Amino Acids*, 2019. **51**: 283–294. doi.org/10.1007/s00726-018-2664-x.

[80] Wzorek A., Sato A., Drabowicz J. *et al*. Remarkable magnitude of the self-disproportionation of enantiomers (SDE) via achiral chromatography; application to the practical-scale enantiopurification of β-amino acid esters, *Amino Acids*, 2016. **48**: 605–613. DOI: 10.1007/s00726-015-2152-5

[81] Kwiatkowska M., Marcinkowska M., Wzorek A. *et al*. The self-disproportionation of enantiomers (SDE) via column chromatography of β-amino-α,α-difluorophosphonic acid derivatives, *Amino Acids*, 2019. **51**: 1377–1385. DOI: 10.1007/s00726-019-02774-7.

[82] Abás S., Arróniz C., Molins E., Escolano C. Access to the enantiopure pyrrolobenzodiazepine (PBD) dilactam nucleus via self-disproportionation of enantiomers. *Tetrahedron*, 2018. **74**: 867–871. doi.org/10.1016/j.tet.2018.01.006.

[83] Terada S., Hirai M., Honzawa A. *et al*. Possible case of halogen bond-driven self-disproportionation of enantiomers (SDE) via achiral chromatography, *Chem. Eur. J*. 2017. **23**: 14631–14638. DOI: 10.1002/chem.201703308.

[84] Sá Gomes P., Rodrigues A.E. Simulated moving bed chromatography: from concept to proof-of-concept. *Chem. Eng. Tech*. 2012. **35**(1): 17–34. doi.org/10.1002/ceat.201100281.

[85] Mazzotti M., Storti G., Morbidelli M. Optimal operation of simulated moving bed units for nonlinear chromatographic separations. *J. Chrom. A*. 1997. **769**(1): 3–24. doi.org/10.1016/S0021-9673(97)00048-4.

[86] Rajendran A., Paredes G., Mazzotti M. Simulated moving bed chromatography for the separation of enantiomers. *J. Chrom. A*. 2009. **1216**(4): 709–738. doi.org/10.1016/j.chroma.2008.10.075.

[87] Hur J.S., Wankat P.C. New design of simulated moving bed (SMB) for ternary separations. *Ind. Eng. Chem. Res*. 2005. **44**(6): 1906–1913. https://doi.org/10.1021/ie040164e.

[88] Kim K.M., Lee J.W., Kim S. *et al*. Advanced operating strategies to extend the applications of simulated moving bed chromatography.

Chem. Eng. Tech. 2017. **40**(12) :2163–2178. https://doi.org/10.1002/ceat.201700206.

[89] Toumi A., Engell S., Diehl M, *et al.* J. Efficient optimization of simulated moving bed processes. Chem. Eng. Process.ing: Process Intensification. 2007. **46**(11): 1067–1084. doi.org/10.1016/j.cep.2006.06.026.

[90] Faria R.P., Rodrigues A.E. Instrumental aspects of simulated moving bed chromatography. *J. Chrom. A*. 2015. **1421**: 82–102. doi.org/10.1016/j.chroma.2015.08.045.

[91] Wu D.J., Xie Y., Ma Z., Wang N.H. Design of simulated moving bed chromatography for amino acid separations. *Ind. Eng. Chem. Res*. 1998. **37**(10): 4023–4035. doi.org/10.1021/ie9801711.

[92] Guest D.W. Evaluation of simulated moving bed chromatography for pharmaceutical process development. *J. Chrom. A*. 1997. **760**(1): 159–162. doi.org/10.1016/S0021-9673(96)00903-X.

[93] Azevedo D.C., Rodrigues A.E. Design methodology and operation of a simulated moving bed reactor for the inversion of sucrose and glucose–fructose separation. *Chem. Eng. J*. 2001. **82**(1–3): 95–107. doi.org/10.1016/S1385-8947(00)00359-4.

[94] Do T.X., Lim Y.I., Lee J., Lee W. Techno-economic analysis of petrochemical complex retrofitted with simulated moving-bed for olefins and aromatics production. Chem. Eng. Res. Design. 2016. **106**: 222–241. doi.org/10.1016/j.cherd.2015.12.020.

[95] Shi Q., Gonçalves J.C., Ferreira A.F., Rodrigues A.E. Simulated moving bed reactor for p-xylene production: Modeling, simulation, and optimization. *Chem. Eng. Scien*. 2020. **225**: 115802. doi.org/10.1016/j.ces.2020.115802.

[96] Mruc P., Olbrycht M., Korbetskyy M., Antos D. Altering the mobile phase composition to enhance self-disproportionation of enantiomers in achiral chromatography. *J. Chrom. A*. 2024. **1715**: 464603. doi.org/10.1016/j.chroma.2023.464603.

[97] Olbrycht M., Gumieniak J., Mruc P. *et al.* Antos, Separation of non-racemic mixtures of enantiomers by achiral chromatography, *J. Chrom. A*. 2023. **1693**: 463877. doi.org/10.1016/j.chroma.2023.463877.

[98] Ziomek G., Antos D., Tobiska L., Seidel-Morgenstern A. Comparison of possible arrangements of five identical columns in preparative chromatography. *J. Chrom. A*. 2006. **1116**(1–2): 179–188. doi.org/10.1016/j.chroma.2006.03.065.

Стаття надійшла 04.02.2025.